CERN-ACC-NOTE-2017-0037

13 June 2017
Miriam.Fitterer@cern.ch

Effect of a resonant excitation on the evolution of the beam emittance and halo population

M. Fitterer, G. Stancari, A. Valishev (Fermilab), R. Bruce,
S. P. Papadopoulou, G. Papotti, D. Pellegrini, S. Redaelli, G. Trad,
D. Valuch, G. Valentino, J. F. Wagner, C. Xu (CERN)

Keywords: electron lens, noise, emittance, halo population

Summary

Collimation with hollow electron beams or lenses (HEL) is currently one of the most promising concepts for active halo control in HL-LHC. In previous studies it has been shown that the halo can be efficiently removed with a hollow electron lens. Equally important as an efficient removal of the halo, is to demonstrate that the core stays unperturbed. In the case of an ideal hollow electron lens without bends, the field at the location of the beam core vanishes and the core remains unperturbed. In reality, the field at the beam core does not vanish entirely due to imperfections in the electron beam profile and the electron lens bends necessary to guide the electron in and out of the proton aperture. In particular, in the case of a pulsed operation of the electron lens the non-vanishing residual field induces noise on the proton beam. To identify the most sensitive pulsing patterns for the resonant mode and derive tolerances on the profile imperfections, a first MD was carried out of which the first results are presented in this note.

Introduction

For high energy and high intensity hadron colliders like the HL-LHC, halo control becomes necessary, for a safe machine operation and control of the targeted stored beam energy in the range of several hundred MJ [1]. Past experiments at the Fermilab Tevatron proton-antiproton collider [2] demonstrated a successful halo control with hollow electron beams or hollow electron lenses (HELs) in DC mode. Simulations of the HEL performance for LHC and HL-LHC [3, 4, 5] show sufficiently high halo removal rate with the HEL operated in DC mode if beams are colliding, but only very low halo removal rates if beams are separated. In order to clean the tails efficiently with the HEL and in a short time-span also in case of separated beams, the halo removal rate can be increased by pulsing the HEL [6, 3, 5], where two different pulsing patterns are considered:

- **random:** the e-beam current is modulated randomly: at every turn the kick is varied between 0 and its maximum value following a uniform distribution,

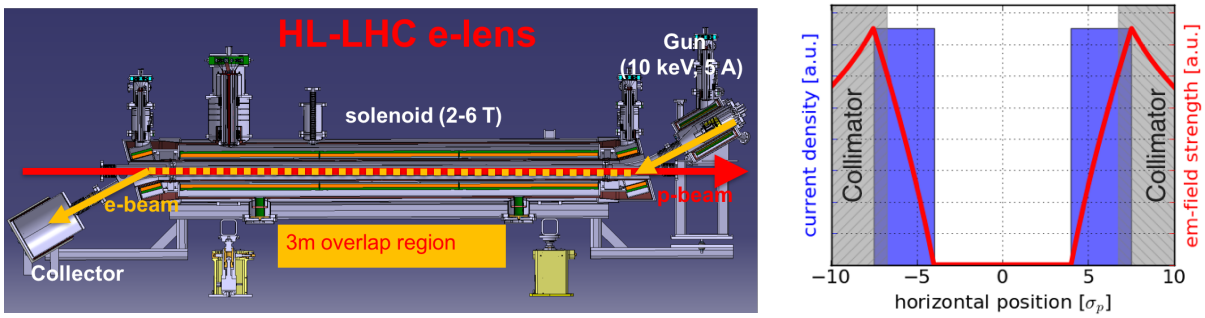

Figure 1: (left) Layout of the hollow electron lens for HL-LHC (left) and sketch of the HEL current density, electromagnetic field strength and collimator aperture for HL-LHC (right).

- **resonant:** the e-lens is switched on only every nth turn with $n = 2, 3, 4, \ldots$ and the maximum kick is applied.

One of the main reservations about pulsing the e-lens is the possibility of emittance growth due to noise induced on the beam core by the HEL. For an ideal radially symmetric hollow electron lens with an S-shaped geometry, the beam core would experience a zero net kick and thus no noise would be induced on the core (see Fig. 1 for the HEL design and for a sketch of the HEL field). In the presence of imperfections in the HEL bends and in the e-beam profile, the kick at the center of the beam is non-zero. First estimates of the residual kick yield 0.5 nrad from the HEL bends assuming 10% difference between entrance and exit bend[1] and 15 nrad due to profile imperfections based on profile measurements of the current HEL e-gun prototype [7]. The estimates for the profile imperfections are likely to be pessimistic as also alignment errors of the solenoids of the test stand and orbit deviations can contribute to the field at the beam center. There is currently an effort ongoing to improve the profile measurements and reduce these effects. In case of DC operation of the HEL the kicks are static and could thus be corrected, if even necessary. However, for a pulsed operation, the tolerable kick amplitudes are much smaller as then noise is introduced also on the beam core. In case of random pulsing, white noise is induced driving all orders of resonances. In case of a resonant pulsing, only certain resonances are driven, explicitly for pulsing every nth turn only the nth order resonances are driven, which can be seen for example from the Fourier series. The nth turn excitation can be represented by

$$f(t) \quad = \quad \sum_{p=-\infty}^{+\infty} \delta(t - p \cdot (nT)), \tag{1}$$

and its Fourier series is then given by:

$$f(t) \quad = \quad \frac{1}{nT} \sum_{k=-\infty}^{+\infty} e^{2\pi i f_k t} \text{ with } f_k = \frac{k}{n} f_{\text{rev}}. \tag{2}$$

[1]Without any imperfections the kick from the e-lens bends at the entrance and exit would compensate each other in case of a S-shaped e-lens and add up in case of an U-shaped e-lens. For the HL-LHC therefore a S-shaped design is chosen. Due to for example field imperfections in the solenoids, space-charge effects or alignment errors, the kick at the entrance and exit can differ. As a first guess a difference of 10% between entrance and exit kick is assumed.

The effect of random noise on the beam has been explored in a previous MD [8] and therefore in this first MD to study the effect on the beam core in case of a pulsed operation only the effect of a resonant excitation was studied. The MD has been performed on 23.08.2016/24.08.2016, fill numbers 5242 and 5243, and different pulsing patterns and excitation amplitudes could be studied during these two fills. Expected effects of the resonant excitation are losses and emittance growth. As experiments at top energy are always not very efficient because of the long recovery times in case of beam dumps, this first try was performed at injection energy. To minimize the emittance growth due to intra-beam scattering, low intensity bunches are used instead of nominal bunches, all other changes were kept to a minimum.

The MD configuration and procedure are described in further detail in Sec. 2, the simulation results are summarized in Sec. 3, and MD results are summarized in Sec. 4.

MD configuration and procedure

MD configuration

In order to keep the machine changes minimal and to also be able to quickly refill the machine in case of beam loss, the MD is conducted with 48 single bunches, single beam and at standard injection settings:

- injection energy (450 GeV), injection tunes $(Q_x, Q_y) = (64.28, 59.31)$
- single bunch intensity: 0.7×10^{11}, number of bunches: 48 (low intensity bunch to minimize emittance growth due to intra-beam scattering)
- normalized emittance: 2.5 μm, bunch length (4 σ): 1.0 ns (use HL-LHC normalized emittance)
- injection optics ($\beta^* = 11$ m), injection tunes
- chromaticity: $Q'_{x/y} = +15$ (standard 2016 settings)
- Landau damping octupole current of $I_{\mathrm{MO}} = \pm 19.6$ A, explicitly +19.6 A for MOF circuit and -19.6 A for MOD circuit (standard 2016 settings)

In order to minimize the emittance blow-up due to intra-beam scattering, a smaller bunch intensity of 0.7×10^{11} is requested for the MD, which leads to about 4.6%/h emittance growth. The lower limit of 0.7×10^{11} is in this case determined by the orbit correction system, for which the BPMs only deliver a good signal for bunch intensities above 0.5×10^{11}. In order to be also more sensitive to the relative emittance growth, the HL-LHC normalized emittance of 2.5 μm is requested which is smaller than the nominal LHC single bunch emittance. Chromaticity and Landau octupole settings have been chosen to comply with the standard 2016 settings at injection. As the resonant excitation is very sensitive to the resonances present, the choice of octupole and chromaticity does have a non-negligible impact on the MD results (see Sec. 3 for a summary of the simulation results and [7] for the complete report).

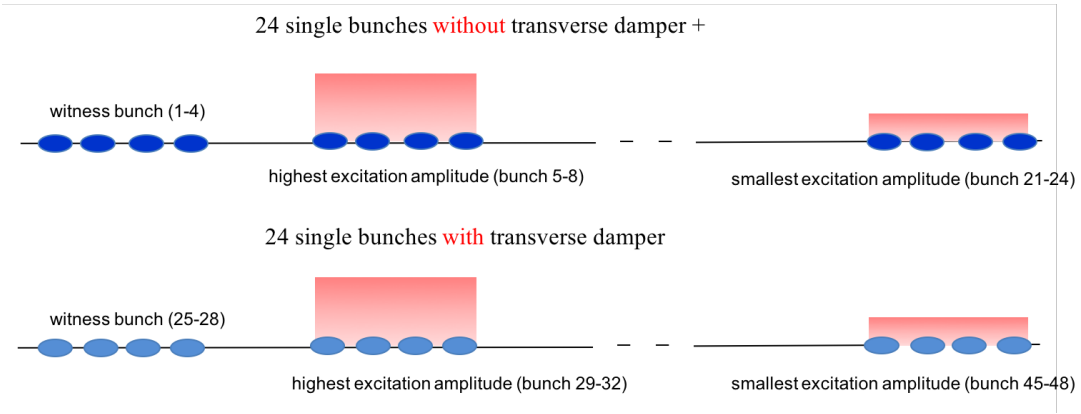

Figure 2: Proposed filling scheme for the MD. For the dark blue bunches (first 24) the transverse damper is not active, for the light blue bunches (second 24) the transverse damper is active. The excitation amplitude indicated with a red rectangle is constant over each group of 4 bunches in order to later be able to increase the statistics by averaging over several bunches. With this filling scheme in total 5 different excitation amplitudes plus the case of no excitation and the cases with the transverse active and not active can be studied during the same fill.

The noise induced by a pulsed e-lens can be approximated to first order by a dipole kick with the corresponding noise pattern/frequency spectrum [7]. In case of the LHC almost arbitrary noise spectra seen by the whole beam can be generated using the transverse damper (ADT) and the amplitude of the noise seen by individual bunches can be controlled by a windowing function placed on top of the generated excitation. Using this method, the kick amplitude is determined very roughly within 50% of the excitation amplitude. The noise patterns can in addition be also changed during the fill. The minimum rise time of the ADT kicker is 700 ns, which determines the minimum bunch spacing required to control the noise amplitude of each individual bunch. By injecting individual bunches the bunch spacing can be chosen between 250 ns to 1 μs [9]. In order to respect the kicker rise time of the ADT and also to avoid multi-bunch instabilities, the MD is conducted with single bunches. Based on these considerations the filling scheme illustrated in Fig. 2 has been chosen for the MD. The filling scheme comprises 2×4 witness bunches (4 with and 4 without transverse damper) and 2×4 bunches per amplitude (4 with and 4 without damper). As each group of 4 bunches experiences the same or no excitation, the statistical significance of the results can be improved by averaging over each group. As the horizontal and vertical kickers of the ADT are not synchronized, exciting the beam in both planes would lead to additional unwanted frequencies. Therefore the excitation is only applied in one plane, where the plane of excitation was chosen so that the expected effect is maximized.

As a first estimate of the kick amplitude, the simulation results were used (see Sec. 3). A strong effect for pulsing every 7th and 10th turn was observed for 120 nrad excitation amplitude and a much smaller effect for any of the other pulsing patterns. No effect was seen for an excitation amplitude of 12 nrad. The simulations also showed that the main effect for pulsing every 7th turn comes from the horizontal excitation and for pulsing every 10th turn the main changes in beam distribution were observed in the

vertical plane, however both vertical and horizontal excitation lead equally to losses and emittance growth. Therefore the horizontal plane was chosen for the 7th turn pulsing and the vertical plane for the 10th turn pulsing. The 8th and 3rd turn were tried in order to test two excitation patterns for which a small/no effect on the beam is expected. In summary, the following pulsing patterns were studied in this MD:

7th turn H plane, 10th turn V plane: to test the two pulsing patterns featuring the largest effect in terms of emittance growth and losses

8th turn H plane: to test one pulsing pattern showing no effect

3rd turn H plane, 3rd turn V plane: the LHC tune is close to the the 3rd order resonances and therefore it is surprising that no strong effect is observed in simulations for this pulsing pattern. If simulations and experiment agree in this case, it is a good confirmation of the simulation model.

MD procedure

The MD consisted of two fills, fill 5242 and fill 5243. During the first fill 5242 different excitation patterns (7th, 8th, 3rd, 10th) were tried. In addition, a first test of the ADT excitation with only pilot bunches was conducted during the first fill for machine protection reasons. The second fill served to obtain an amplitude scaling for pulsing every 10th turn with an unperturbed initial beam distribution. The detailed time line is summarized in Table 1.

Table 1: Time line and list of excitation patterns and amplitudes during the MD. Times are given in Europe/Zurich time.

fill number	time	pulsing pattern [turns]	plane	amplitude [nrad]
5242	23:23	testing with probes		
	23:23 – 00:56	setup machine, inject 48 bunches		
	00:56 – 00:58	testing with 48 bunches (7th, H, 6 nrad)		
	00:58 – 01:21	no excitation, let distribution adjust		
	01:21 – 01:40	7	H	6
	01:40 – 01:50			12
	01:50 – 02:04			24
	02:05 – 02:14	8	H	24
	02:14 – 02:15	3	H	6
	02:15 – 02:16			12
	02:16 – 02:21			24
	02:29 – 02:31	3	V	12
	02:31 – 02:37			24
	02:38 – 02:41	10	V	24
	02:41 – 02:52			48
	02:53 – 02:54			72
	02:54 – 02:57			96

(The table continues on the next page)

(Table continued from previous page)				
fill number	time	pulsing pattern [turns]	plane	amplitude [nrad]
5243	03:11 – 03:34	setup machine, inject 48 bunches		
	03:34 – 03:46	no excitation, let distribution adjust		
	03:46 – 03:57 03:57 – 04:08	10	V	48 96

Summary of simulation results

In preparation of the MD, simulations with the tracking code Lifetrac [10] have been performed, which are summarized in more detail in [7].

The experimental scenario has been modeled using the current MAD-X mask files used for SixTrack studies which are then exported to Lifetrac. Two scenarios, one with and one without magnetic errors, have been used in order to study the impact of the magnetic errors[1]. The comparison with and without errors is particularly relevant as the resonant excitation is based on the excitation of specific resonances and with these two cases it can be identified if the effect is due to magnetic errors or already from the clean machine with linear elements, sextupoles and octupoles. Different pulsing patterns up to pulsing every 10th turn in both transverse planes have been simulated in order to compare the different pulsing patterns. However, in the MD the excitation is only applied in one plane at a time as the ADT horizontal and vertical kickers are not synchronized and additional frequencies would thus be introduced in case of a pulsing in both transverse planes. In order to compare with the MD results, the simulations have then been repeated for 7th turn pulsing H and 10th turn pulsing V including also additional excitation amplitudes in order to obtain a scaling of the losses and emittance growth with amplitude.

Without machine imperfections, pulsing in H+V, 120 nrad

Without errors, an effect of the excitation is only observed for pulsing every 7th and 10th turn in terms of:

- beam losses and a simultaneous decrease of the bunch length indicating longitudinal losses,
- an adjustment of the beam distribution over 10^4 turns to a steady distribution with increased emittance.

The strong effect for pulsing every 7th and 10th turn can be explained by an excitation of the 7th and 10th order resonances driven by the strong sextupoles (see the FMA analysis in Fig. 3). The octupoles serve the purpose of providing the tune spread. The (mainly longitudinal) losses are due to the high chromaticity, as the synchrotron motion and the chromatic detuning lead to a repeated crossing of the off-momentum particles

[1] In this model also linear errors, explicitly a_1, a_2, b_1, b_2 are included. The strength of the linear errors is adjusted in order to obtain around 1 mm rms orbit deviation and 15 % peak beta-beat.

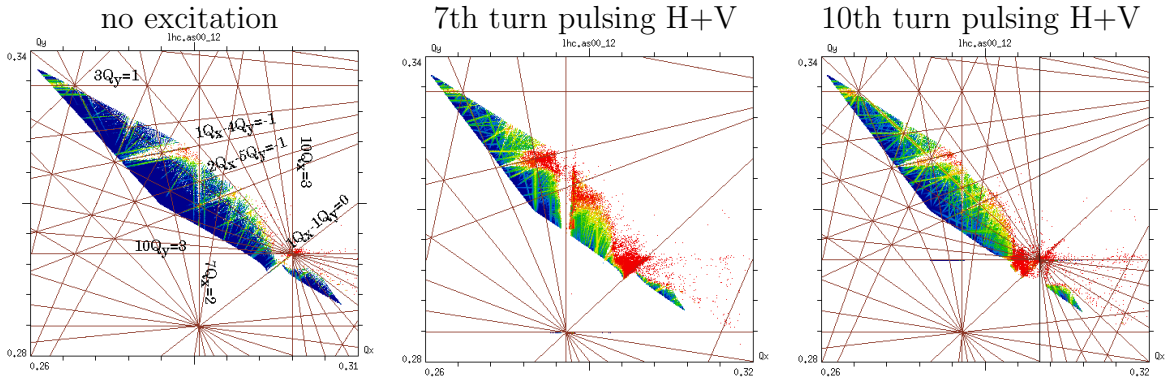

Figure 3: Scenario without machine errors, excitation amplitude 120 nrad: FMA analysis with Lifetrac for on-momentum particles ($\frac{\Delta p}{p_0} = 0$) up to 8 σ amplitude for a square grid: no excitation (left), pulsing every 7th turn (center) and pulsing every 10th turn (right).

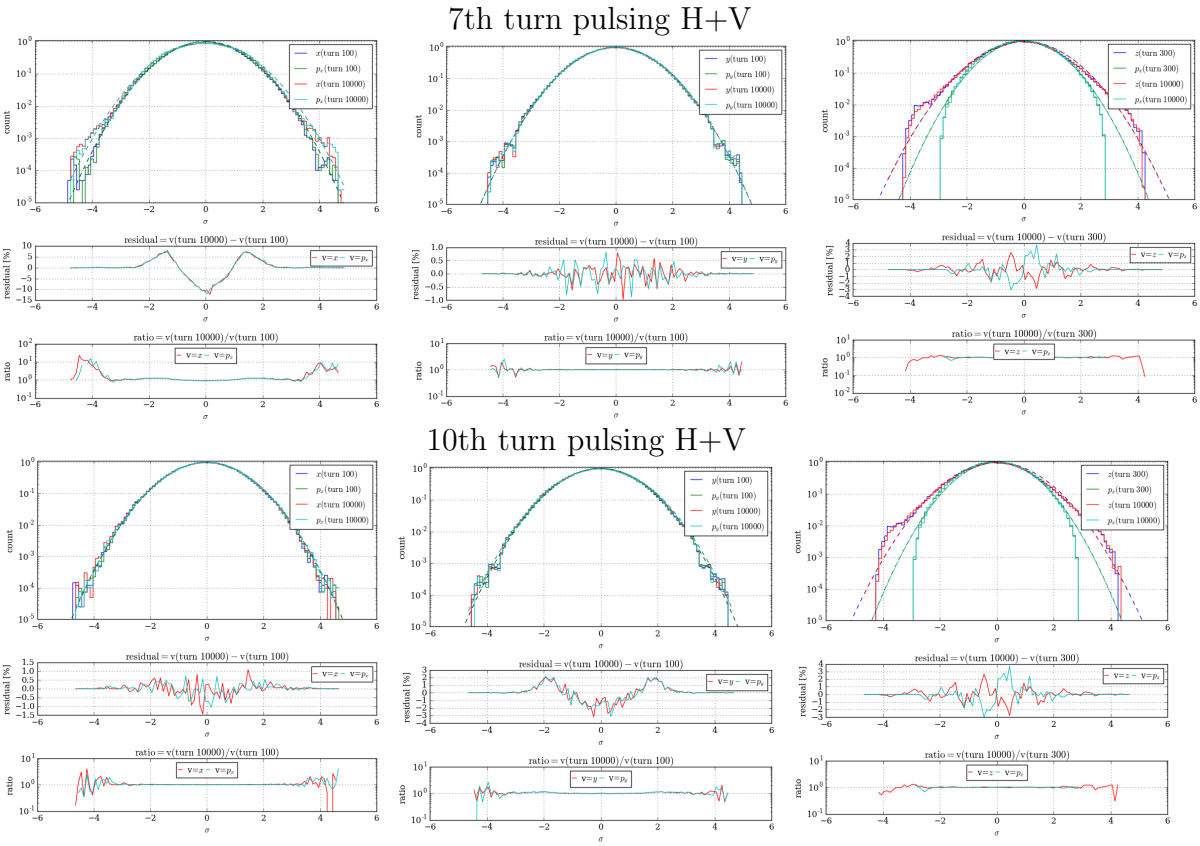

Figure 4: scenario without machine errors, excitation amplitude 120 nrad: Normalized amplitude distribution in (x, p_x) (left), (y, p_y) (center) and (z, p_z) (right) for pulsing every 7th (top) and 10th turn (bottom) in H and V. The initial distributions after equilibration (around 100 turns) and the distribution after the fast change (10 000 turns) are compared. The residual is in general sensitive to changes in the beam core and middle while the ratio is sensitive to changes in the high-amplitude tails.

over the resonances. The adjustment of the beam distribution over the first 10^4 turns is illustrated in Fig. 4, which compares the initial beam distribution with the one observed after 10^4 turns. The following changes in distribution can be observed:

7th turn H+V For pulsing every 7th turn in H+V, the distribution only changes in the *horizontal* plane, explicitly:

- depletion of the center of the core and increase of the density between 1.8–2.0 σ.
- increase of the tail population around 4 σ

10th turn H+V For pulsing every 10th turn in H+V, the distribution only changes in the *vertical* plane, explicitly:

- depletion of the center of the core and increase of the density between 2.0–2.2 σ.
- no increase of the tail population

The change of the longitudinal distribution is due to the small initial mismatch of the distribution as the initial distribution matching does not take the non-linearity of the bucket into account.

With machine imperfections, pulsing in H+V, 120 nrad

With machine imperfections, the strongest effect is also observed for pulsing every 7th and 10th turn. The main effect thus originates from the strong sextupoles and octupoles and high chromaticity. The initial increase in emittance is due to the fast change of the beam distribution over the first 10^4 turns, so the first point in these simulations is already after the initial adjustment of the distribution. The losses are now not only longitudinal, but also transverse observable as a decrease in transverse emittance and bunch length. In addition, also other excitation patterns – mainly every 3rd turn – show losses due to the magnetic errors (up to 14th order are included in the simulation). A quantitative comparison of the losses is shown in Fig. 5 and the obtained emittance, bunch length and losses are shown in Fig. 6.

With machine imperfections, pulsing in H+V, 12 nrad

The simulation results presented in Sec. 3.1 and 3.2 were performed for an excitation amplitude of 120 nrad and pulsing in the horizontal and vertical plane (H+V). A reduction of the amplitude by a factor 10, i.e. 12 nrad, shows no observable effects on the beam core, even with machine imperfections. The limit from simulations on the maximum excitation amplitude for which the beam will stay unperturbed must thus lie within 12 nrad and 120 nrad.

MD scenario: with machine imperfections, pulsing 7th turn H, pulsing 10th turn V

During the MD a significant effect was observed for pulsing every 7th turn H and 10th turn V. For the other pulsing patterns (8th turn H, 3rd turn H, 3rd turn V) no effect was

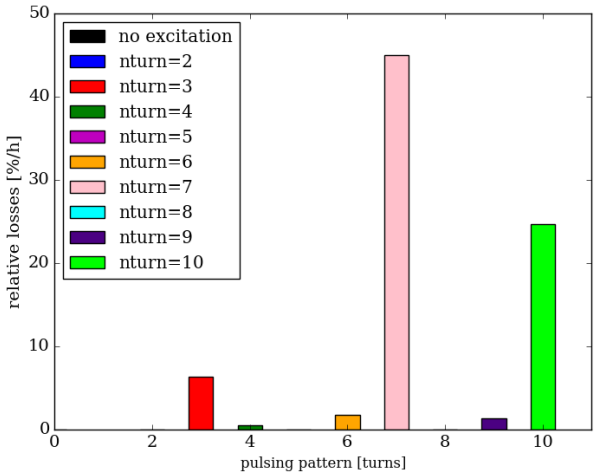

Figure 5: scenario with machine imperfections, excitation amplitude 120 nrad: Relative losses over 10^6 turns $((I_{\text{initial}} - I_{\text{final}})/I_{\text{initial}})$ converted to a loss rate per hour. The largest losses are observed for pulsing every 7th and 10th turn.

observed. The beam distribution was however already so perturbed for these cases, that for a conclusive result, these cases have to be tested again in a future MD. In addition, the excitation could only be applied in one plane in the MD, as the ADT kickers in H and V are not synchronized. Losses were also observed already for significantly smaller excitation amplitudes, explicitly for maximum excitation amplitudes of 6 nrad for 7th H and 48 nrad for 10th V. In order to compare with the MD results, a scan in excitation amplitude for pulsing every 7th turn *only* in H and every 10th turn *only* in V have been performed and the results are shown in Fig. 7 together with the simulations for pulsing in H and V.

For pulsing every 7th turn, the main effect is due to the pulsing in the horizontal plane as:

- the loss rate is only slightly smaller for pulsing only in H compared to pulsing in H+V
- for pulsing only in V, no losses are observed at all

For pulsing every 10th turn, both planes contribute equally and pulsing in both planes might excite in addition some coupling resonances as:

- the loss rates for pulsing only in H and only in V are similar
- the loss rate for pulsing in H+V is considerably higher than only pulsing in one plane

As also seen in the other simulations, the main change of the beam distribution for pulsing only in one plane takes place during the first 10^4 turns. This change is illustrated in Fig. 8 which compares the initial beam distribution and the distribution after 10^4 turns for the case of pulsing every 7th turn H and 10th turn V. Same as for pulsing in H+V, a change in beam distribution is only observed in the horizontal plane for 7th turn H and in the vertical plane for 10th turn V. However the changes in beam distribution are slightly different:

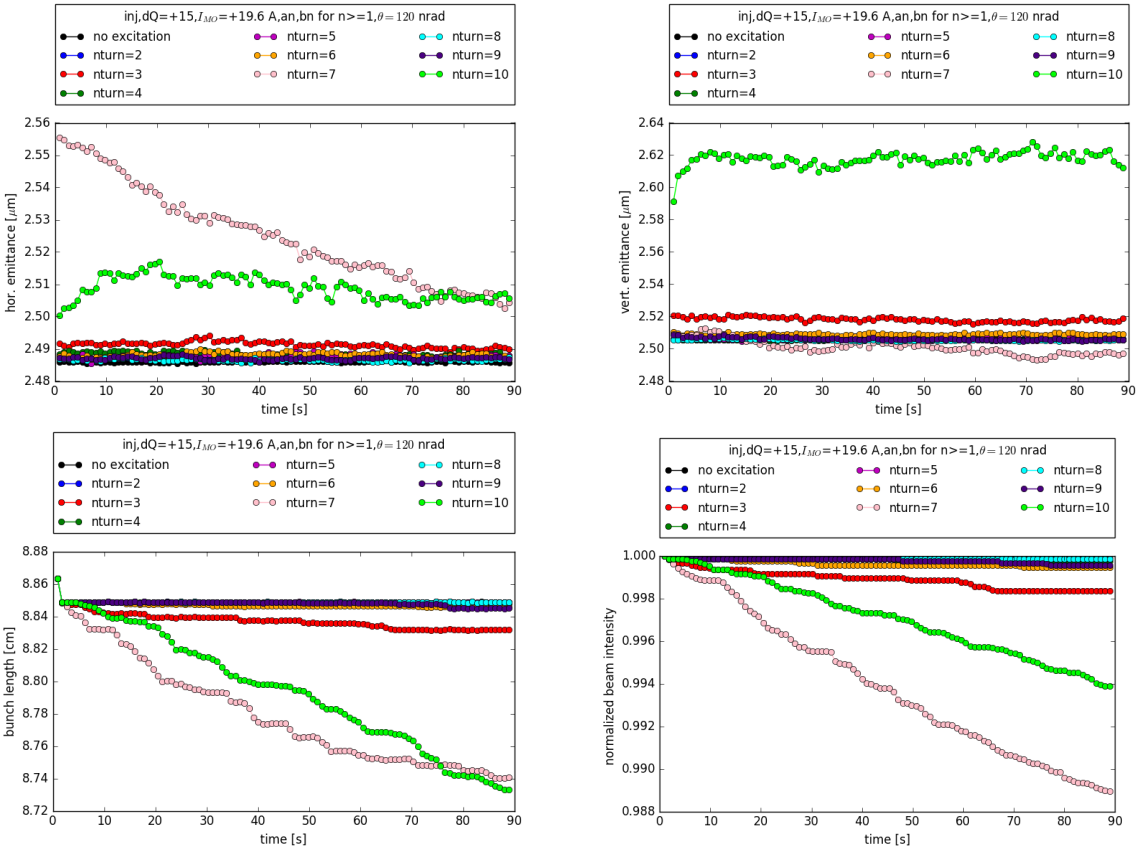

Figure 6: scenario with machine imperfections, excitation amplitude 120 nrad: Hor. (top left) and vert. (top right) normalized emittance and 1σ rms bunch length (bottom left) and normalized beam intensity (bottom right) over 10^6 turns. A change in emittance is observed for pulsing every 7th and 10th turn and to a smaller extent for pulsing every 3rd turn. The large initial increase in emittance for pulsing every 7th and 10th turn is due to a change in beam distribution which takes place over the first 10^4 turns.

7th turn H: the depletion in the core is less pronounced and the increase in the middle (around 1.8 σ) of the beam distribution is moved towards higher amplitudes. In summary an increase of the tails is observed starting from around 2.2 σ and with a maximum around 3.0 σ.

10th turn V: the main increase of the distribution is observed around 1.5 σ for pulsing only in V compared to 2.0 σ for H+V. The depletion in the core is also more concentrated in the center of the beam for pulsing only in H (within $\pm$0.5 σ) compared to pulsing in H+V, where the core is depleted within $\pm$1.1 σ

Results

During the MD the bunch-by-bunch beam losses were recorded with the Fast Beam Current Transformer (FBCT) and the diamond detectors. In this note only the FBCT measurements are analyzed. The emittance was measured using the Beam Synchrotron

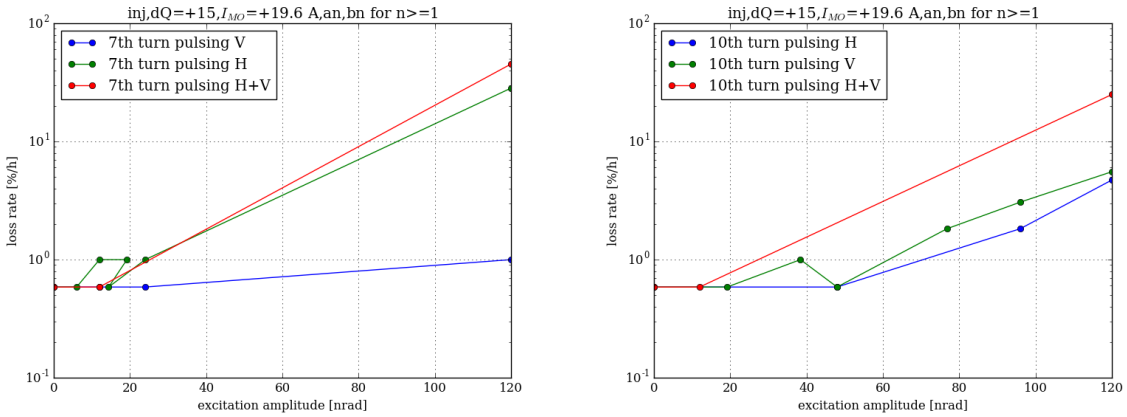

Figure 7: scenario with machine imperfections and different excitation amplitudes: Normalized beam intensity for pulsing every 7th turn (left) and 10th turn (right). Particles have been tracked over 10^6 turns. For pulsing every 7th turn the main effect originates from the excitation in H, while for pulsing every 10th turn, both planes appear to be equal.

Radiation Telescope (BSRT) and the wire scanners. In addition to the emittance measurements, also the horizontal and vertical BSRT profiles were recorded in order to obtain more information about eventual changes in the beam distribution and a summary of the analysis of these profiles is given in the following preceded by a short introduction to the BSRT profile analysis in Sec. 4.1. Another method to obtain information about the tail distribution is to operate the wire scanners with increased gain, so that the profiles are more sensitive in the tail region while being saturated in the core region. The data was recorded during the MD, but unfortunately no useful results could be extracted in a first attempt.

In this section, the results are presented in chronological order for the different pulsing patterns (see Table 1 for the time line). Detailed descriptions of the definitions and analysis are only given in the first analysis (Sec. 4.2.1). For each pulsing pattern the following analysis is performed:

1. analysis of loss rates using the bunch-by-bunch intensity measured with the FBCTs

2. analysis of the normalized bunch-by-bunch emittance measured with the BSRT and as logged in the LHC logging database. In this case, the emittance is obtained via an automatic Gaussian fit to the profiles.

3. in detail analysis of the BSRT profiles by calculating different statistical parameters and comparing the evolution of the profiles with time. A summary of the analysis is given in Sec. 4.1 and more details of the BSRT profile analysis can be found in [11].

In general it should be kept in mind, that the beam distribution is only unperturbed before the first excitation and first maximum excitation amplitude, which is for fill 5242 every 7th turn H with an excitation amplitude of 6 nrad. In fill 5243 only one excitation pattern was studied, every 10th turn V, but different amplitudes were tried. The first case studied for fill 5243 is 10th turn V with an excitation amplitude of 48 nrad.

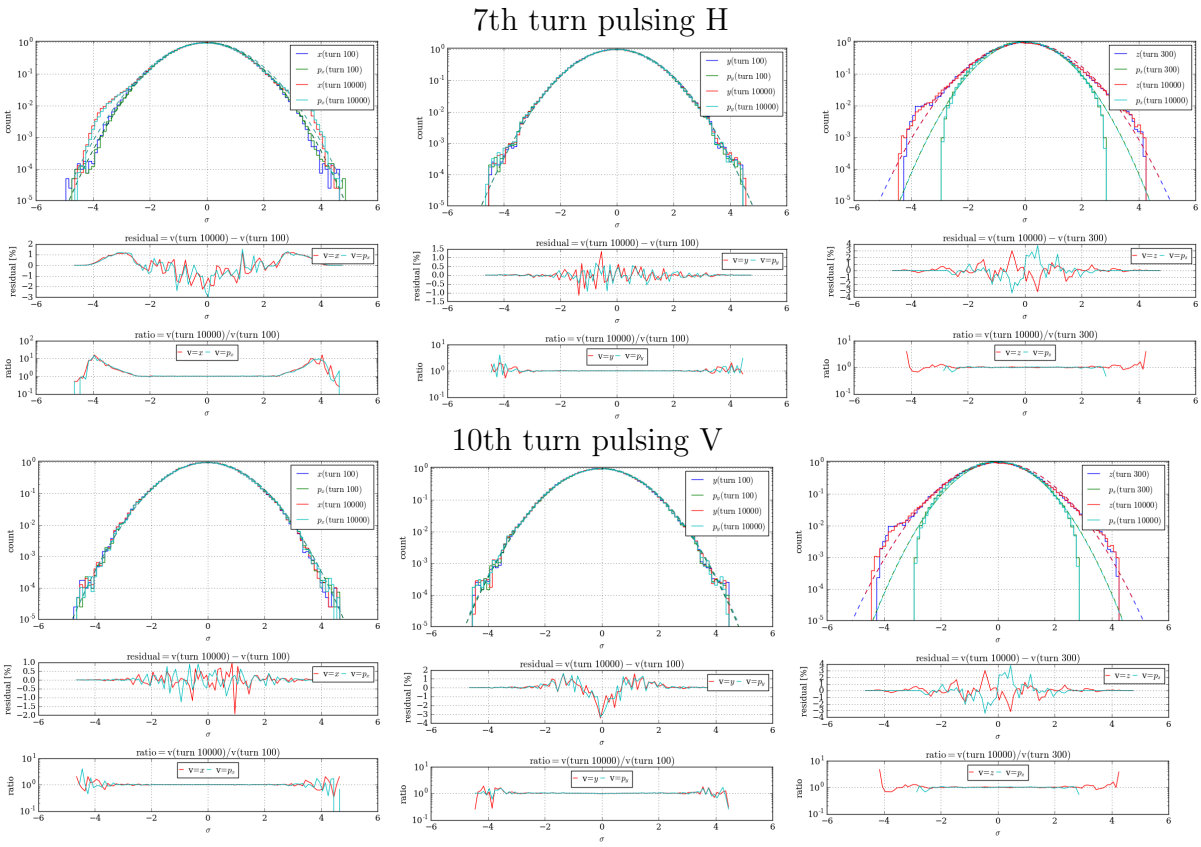

Figure 8: scenario with machine errors, excitation amplitude 120 nrad: Normalized amplitude distribution in (x, p_x) (left), (y, p_y) (center) and (z, p_z) (right) for pulsing every 7th turn H (top) and 10th turn V (bottom). The initial distributions after equilibration (after around 100 turns) and the distribution after the fast change (after 10 000 turns) are compared.

BSRT profiles at injection

This chapter intends to give a short overview of the BSRT profile analysis presented in this note. For a more detailed description of the analysis, it is referred to [11]. The BSRT image formation is mathematically described as a convolution of the beam distribution with the optical resolution (LSF). Assuming that the beam distribution as well as the optical resolution (LSF) are Gaussian a conversion factor $c_{\mathrm{LSF},z}$ ("LSF factor") can be derived which is nothing else than the width of the Gaussian distribution of the optical resolution[1]:

$$\sigma_{\mathrm{beam},z} = \sqrt{\sigma^2_{\mathrm{profile},z} - c^2_{\mathrm{LSF},z}}, \quad z = h, v. \tag{3}$$

The position can then be very roughly also be expressed in beam sigma:

$$z[\sigma_{\mathrm{beam},z}] = \frac{z[\mathrm{mm}]}{\sigma_{\mathrm{beam},z}[\mathrm{mm}]}, \quad z = h, v. \tag{4}$$

[1]The convolution of two uni-variate Gaussian distributions f and g having respectively the means μ_f and μ_g and standard deviation σ_f and σ_g is a Gaussian distribution with mean and standard deviation $\mu_{f*g} = \mu_f + \mu_g$ and $\sigma_{f*g} = \sqrt{\sigma_f^2 + \sigma_g^2}$

The BSRT profiles are in general a projection of the BSRT synchrotron light black and white image projected on the horizontal and vertical axis. The result are histograms in both planes representing the projections of the horizontal/vertical bunch distribution. The BSRT can take images of only one bunch at a time and in order to record all bunches during one fill the device loops through the individual bunches. For each time stamp several profiles of the same individual bunch are taken. In this MD, explicitly three profiles of one individual bunch were taken for each time stamp (see profile 1–3 in green and blue in Fig. 9). Using these profiles, the general steps in the analysis are:

1. The profiles are converted to probability distributions $\rho(x)$ by dividing the bin height by the integral over the profile, so that:

$$\int_{-\infty}^{\infty} \rho(x) = 1 \tag{5}$$

2. The background is calculated by averaging the first and last ten bins of all profiles for each individual bunch over the complete time of acquisition. This constant is then subtracted from the normalized distribution. After the background subtraction, the profiles are renormalized so that the integral over the distribution is one. The profiles are checked before and after background subtraction, as this can hide real physical effects or also introduce artificial features.

3. The profiles are averaged in order to reduce the noise. Explicitly the profiles are averaged in two different ways:

   - the three profiles of each individual bunch are averaged for each time stamp ("average profile")
   - the moving average and standard deviation over 11 time stamps ("moving average profile") is taken. Thus with three profiles per time stamp in total 33 profiles are averaged. The obtained standard deviation for each bin is used as an estimate for the error in each bin. These estimated errors are then used as weights for the least square fit of the Gaussian and q-Gaussian distribution and for the calculation of the chi-squared as a measure of the goodness of the fit. The moving average profile is shown as a black line in Fig. 9.

4. A Gaussian (light red dashed line in Fig. 9) and q-Gaussian distribution (dark red line in Fig. 9) are fitted to the average profile and the moving average profile. In case of the moving average profile, the fit is weighted with the calculated standard deviation for each bin.

   The Gaussian distribution is defined as

$$f_{\text{Gauss}}(x) := c + a \cdot \frac{e^{-\frac{(x-\mu)^2}{2\sigma^2}}}{\sqrt{2\pi}\sigma}, \tag{6}$$

   where μ is the mean and σ the standard deviation of the distribution.

   The q-Gaussian distribution is defined as

$$f_{\text{q-Gauss}}(x) = c + a \cdot \frac{\sqrt{\beta}}{C_q} e_q(-\beta(x-\mu)^2), \tag{7}$$

where μ is the mean of the distribution and

$$e_q(x) = (1 + (1-q)x)^{\frac{1}{1-q}} \tag{8}$$

is the q-exponential. The normalization factor C_q is given by

$$C_q = \frac{\sqrt{\pi} \cdot \Gamma\left(\frac{3-q}{2(q-1)}\right)}{\sqrt{q-1} \cdot \Gamma\left(\frac{1}{q-1}\right)}, \text{ for } 1 < q < 3, \tag{9}$$

For $q < \frac{5}{3}$ the standard deviation σ is then given by:

$$\sigma^2 = \frac{1}{\beta(5-3q)} \tag{10}$$

For other values of q the standard deviation is either infinite or not defined. The range of the parameter q is limited to $0 < q < 3$. The parameter q is an estimator for the tail population. For $q \to 1$ the Gaussian distribution is recovered, for $q > 1$ the distribution features heavier tails compared to the Gaussian distribution and for $q < 1$ lighter tails. The parameter c is introduced in the Gaussian and q-Gaussian fit in order to model the background of the profiles implying the introduction of the parameter a in order to fulfill the requirement that the integral over the distribution is one.

5. statistical parameters are calculated for the average and moving average profile, including the cumulative sum of the distribution shown in Fig. 9 lower right.

6. To better visualize the changes of the distribution, the residual Res and the ratio Rat for bunch i at time stamp t_i in respect to reference bunch j at time stamp t_j are calculated with

$$\text{Res}(t_i, x) = A_i(t_i, x) - A_j(t_j, x) \tag{11}$$

$$\text{Rat}(t_i, x) = \frac{A_i(t_i, x)}{A_j(t_j, x)} \tag{12}$$

where $A_i(t_j, x)$ denotes the amplitude at bin x of bunch i at time stamp t_j. In this MD the residual and ratio are taken in respect to the initial distribution of the bunch itself, explicitly:

$$\text{Res}(t_i, x) = A_i(t_i, x) - A_i(t_j, x) \tag{13}$$

$$\text{Rat}(t_i, x) = \frac{A_i(t_i, x)}{A_i(t_j, x)} \tag{14}$$

The residual is in general sensitive to changes in the core region and the ratio to changes in the tails. The residual proved to be a good indicator for changes in the core while the ratio turned out to be too sensitive to the noise of the BSRT profiles.

A typical bunch distribution for a reference bunch without any excitation is shown in Fig. 9.

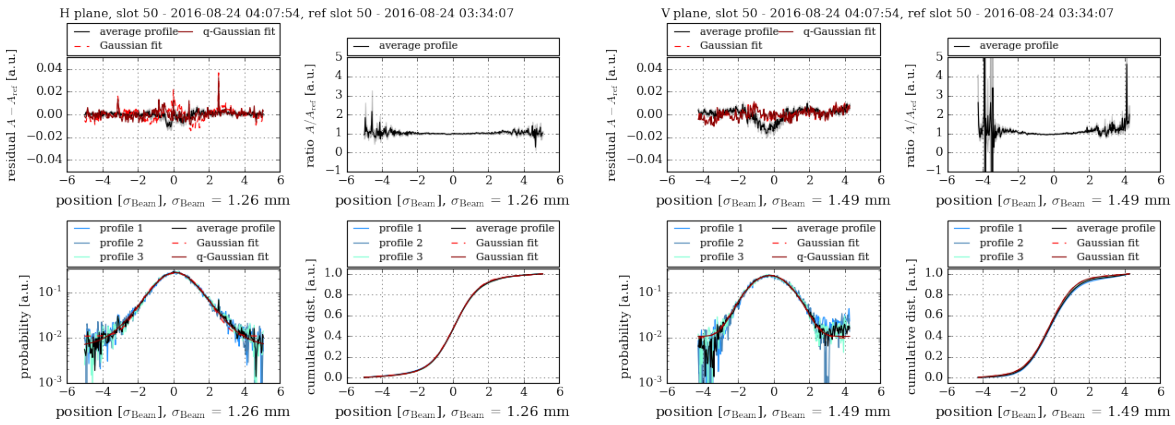

Figure 9: Typical BSRT profile at injection for the horizontal (left) and vertical (right) plane. The profile was taken towards the middle of fill 5243 (2016-08-24 04:08:36) and for a bunch not experiencing any excitation. For this bunch, the transverse damper is not active. Similar profiles are obtained also for the bunches with transverse damper active. The residual and ratio are taken in respect to a profile at the beginning of the fill (2016-08-24 03:34:07). The background is not subtracted and the moving average profiles are shown as black line in all subplots. For the moving average the profiles are explicitly averaged over 11 time stamps with 3 profiles per time stamp. Note that the x-axis is the position of the BSRT image projection and *not* the proton beam sigma. The raw profiles for this time stamp are shown in blue and green in the probability distribution (lower left) and cumulative sum (lower right). For the residual and ratio the moving average profile is shown in black together with the 1σ standard deviation over the 11 time stamps as gray envelope. The Gaussian fit is shown in dashed red and the q-Gaussian fit in solid dark red in the profile plot (lower left) and the deviation from the fit with the same color coding in the residual plot (upper left).

The following observations can be maid:

- The distribution in the *horizontal* plane features over-populated tails and the q-Gaussian fit represents a better model for the distribution. The tails are slowly depleted during the fill as illustrated in Fig. 10 showing a decrease of q starting from $q \approx 1.3 - 1.35$ for all bunches.

- The distribution in the *vertical* plane has slightly underpopulated tails as $q \approx 0.97 < 1$ (see Fig. 10). The q-parameter stays unchanged indicating that the shape of the distribution stays unchanged.

- The distribution shows a "bump" on the right side (positive position) of the horizontal profile and left side (negative positions) of the vertical profile. A possible explanation for the bump could be a spot in the image. Note that the bump is not well visible in Fig. 9.

- There are strong oscillations of the distribution during the fill mostly visible as fluctuation in the residual of the distribution. By averaging over several profiles as done in the moving average, the fluctuations can be reduced.

- The cumulative sum (CDF) of the distribution is a smooth function for both planes and can be used to define a model independent definition of the standard deviation σ of the distribution [1]. Based on the analogy of the cumulative distribution function and the standard deviation for a Gaussian distribution we define the standard deviation σ as:

$$\sigma_{32} = \mathrm{CDF}^{-1}(0.32) \tag{15}$$
$$\sigma_{68} = \mathrm{CDF}^{-1}(0.68) \tag{16}$$

  The left and right side are calculated separately because of the bumps in the BSRT distribution on the left for the vertical and right for the horizontal.

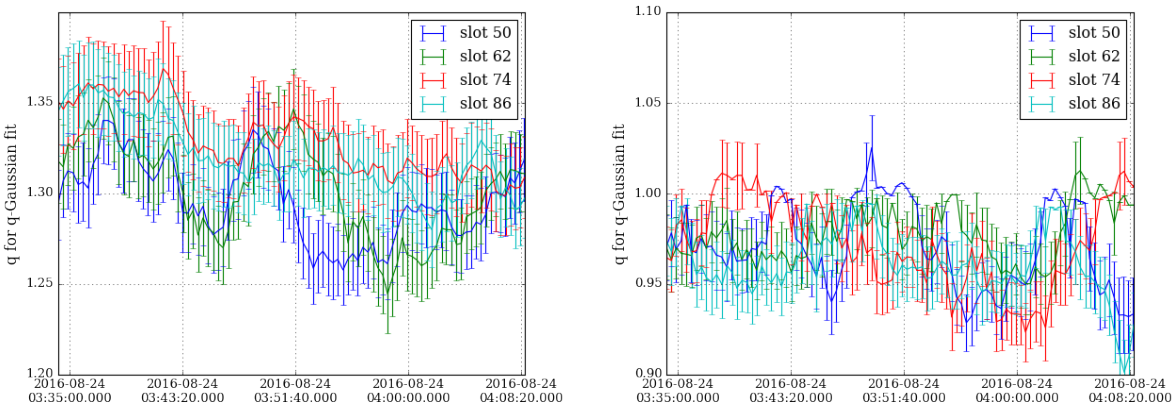

Figure 10: q parameter of q-Gaussian fit in the horizontal (left) and vertical (right) plane: q-parameter for four references bunches not experiencing any excitation during fill 5243 and with the damper not active. The q-Gaussian fit is performed for the moving average profiles and without background subtraction. The errorbars contain only the error from the q-Gaussian fit obtained from the covariance matrix ($\sigma_q = \sqrt{(\mathrm{cov}(p_q, p_q)}$ where p_q indicates the diagonal element of the matrix for the fit parameter q). In the vertical plane the fit did not always converge and for better visibility the large error bars are in this case replaced with 0. In the horizontal plane the tails are clearly overpopulated in respect to a Gaussian distribution as $q > 1$ and slowly depleted during the fill visible as a slight decrease of q. In the vertical plane, the tails are underpopulated as $q < 1$ and stay more or or less constant.

Fill 5242, 7th turn H

In the following sections the analysis of the FBCT and BSRT measurements are presented. Preceding the analysis it should be noted that the BSRT profile analysis revealed a change

[1]The BSRT emittance obtained from the LHC logging database (see Sec. 4.2.2) is the sigma of the distribution obtained via a Gaussian fit to the distribution assuming that a Gaussian fit is a well suited model. For example in the horizontal plane the tails are over-populated and the Gaussian distribution does not represent a good model.

in beam distribution in the horizontal and vertical plane also for the reference bunches around 01:30:00, just in the middle of the excitation with 6 nrad maximum excitation amplitude. This change in distribution complicates the BSRT emittance and profile analysis as it is then not obvious if the change in distribution is due to the excitation or not. A correlation of this change in distribution with the loss rate or emittance could however not be found.

Losses and loss rates from FBCT measurements

To calculate the relative averaged bunch intensity losses, the measured bunch intensity I is first normalized to the initial intensity I_0. The relative losses $I_{\mathrm{lost},j}$ for each individual bunch are then given by:

$$I_{\mathrm{lost,j}} = 1 - \frac{I_j}{I_{j,0}},\ j = 1, \ldots, 48$$

The average is then taken over the bunches with the same excitation amplitude:

$$I_{\mathrm{lost}}(n \cdot \Delta A) = \frac{1}{4} \cdot \sum_{j=\text{bunches with } n\cdot\Delta A} I_{\mathrm{lost,j}}. \tag{17}$$

Fig. 11 shows the relative bunch intensity losses measured with the FBCT averaged over the bunches with the same excitation amplitude as defined in Eqn. 17. The losses clearly depend on the excitation amplitude and the transverse damper does not change the loss rate significantly.

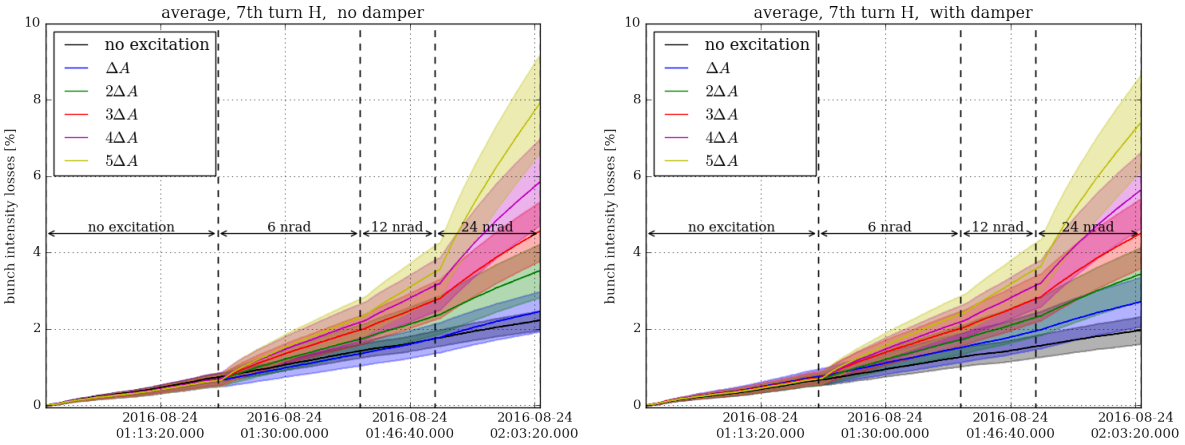

Figure 11: 7th turn pulsing H: Relative bunch intensity losses measured with the FBCTs (Eqn. 17). The average over the group of four bunches experiencing the same excitation amplitude is indicated by a solid line together with the 1σ standard deviation over the four bunches indicated as an envelope in the same color. The maximum excitation amplitudes are indicated with black arrows. A clear increase of the losses with excitation amplitude within the bunch train ($n \cdot \Delta A$) and at each increase of the maximum amplitude (A_{max}) is visible.

A quantitative comparison of the loss rate for the three different maximum excitation amplitudes ($A_{\mathrm{max}} = 6$ nrad, $A_{\mathrm{max}} = 12$ nrad, $A_{\mathrm{max}} = 24$ nrad) is shown in Fig. 12, where

the loss rate is defined as

$$L_{\text{loss}}(n \cdot \Delta A) := < \frac{I_{\text{start excitation}} - I_{\text{end excitation}}}{I_{\text{start excitation}} \cdot \Delta t_{\text{excitation}}} >_{\text{bunches with } n \cdot \Delta A} \tag{18}$$

and the average is taken over the bunches with the same excitation amplitude $n \cdot \Delta A$. As the duration of the excitations differs for the different maximum excitation amplitudes A_{max}, it is better to compare loss rates instead of relative losses. However, the loss rate as defined in Eqn. 17 does not distinguish between initial losses due to an initial depletion of the tails occurring when the excitation is switched on and continuous losses due to diffusive processes caused by the excitation. This explains the general decrease of the loss rates with the maximum excitation amplitude A_{max}. During the first excitation, here $A_{\text{max}} = 6$ nrad, the initial tails are slowly depleted. The following excitations ($A_{\text{max}} = 12$ nrad and $A_{\text{max}} = 24$ nrad) then exhibit smaller loss rates as they start already from a depleted distribution. The loss rate for one maximum excitation amplitude A_{max} in general scales quadratically with the excitation amplitude $n \cdot \Delta A,\ n = 0, \ldots 5$ indicated by a quadratic fit in Fig. 12.

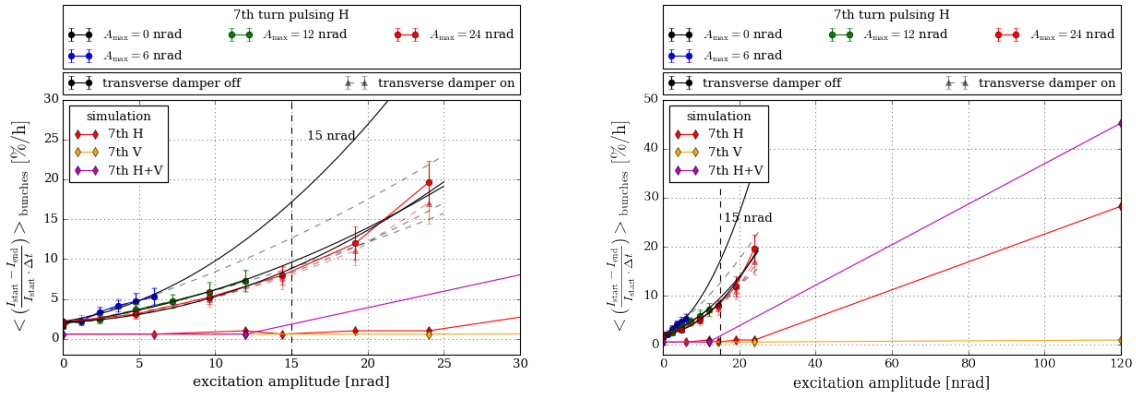

Figure 12: 7th turn pulsing H: Average bunch intensity loss rate measured with the FBCTs (Eqn. 18) together with the loss rates obtained in Lifetrac simulation (see Sec. 3.4). The left plot is a zoom of the right plot. The measurements for the different maximum excitation amplitudes A_{max} are indicated in different colors. The bunches for which the transverse damper is active are shown with solid dots and the bunches for which the transverse damper is not active are shown with slightly transparent triangles. Each point represent the average over the four bunches with the same excitation amplitude $n \cdot \Delta A$. The loss rates obtained in Lifetrac simulations are indicated with diamonds (see Sec. 3). Note that losses are actually only observed at higher excitation amplitudes in simulations, which is visible only on the zoomed out right plot. The loss rates follow in general a quadratic behavior. The second order polynomial fit to the loss rate is indicated with a solid line for the bunches with transverse damper active and with a dashed line for the bunches with the transverse damper not active. The vertical dashed line at 15 nrad indicates the expected kick amplitude from the LHC electron lens [7].

Fig. 12 also shows the loss rates obtained from Lifetrac simulations (see Sec. 3). In the simulations the collimation system is simulated as a single black absorber with an

aperture of 6 beam σ and a normalized beam emittance of 2.5 μm. In the MD the TCPs were set at 5.7 σ assuming 3.5 μm normalized beam emittance. As the aperture in simulations is much smaller than in the MD in general higher losses were to be expected in the MD. On the contrary, the loss rates from simulations are much smaller than the experimental ones. The difference can also not be explained by the 50% error in the excitation amplitude of the ADT (see Fig. refres:fig:7H:2). Explanation for a smaller loss rate are:

- no diffusive processes like e.g. intra-beam scattering are taken into account in the simulations. The only diffusive process in the simulations are actually non-linearities and the negligible numerical noise.
- only one seed has been simulated and for a statistically valid simulation, at least the average over a few seeds should be taken.

However, the magnitude of the difference is surprising and should be considered in the future.

At last, we want to compare the loss rates obtained in the MD to the kick amplitudes expected for a hollow electron lens. From measurements of the 1-inch hollow electron gun prototype, the expected dipole kick amplitude from profile imperfections and from the electron lens bends on particles in the center of the beam is estimated to be [7]:

$$\theta = 15 \text{ nrad}$$

where the main contribution comes from profile imperfections. This value of 15 nrad is indicated with a black dashed line in Fig. 12 and the estimated loss rates L_{loss} from the MD using the second order polynomial fit $a + b \cdot x + c \cdot x^2$ for extrapolation/interpolation to 15 nrad are summarized in Table 2. The loss rates for 15 nrad lie in general between 8 %/h and 17 %/h.

Table 2: 7th turn pulsing H: Loss rate L_{loss} as defined in Eqn. 18 for the kick amplitude expected from a hollow electron lens on the core particles $A = 15$ nrad. The values for 15 nrad excitation amplitude are extrapolated/intrapolated from the second order polynomial fit to the loss rate for the different maximum excitation amplitudes A_{max} (see Fig. 12).

A_{max} [nrad]	L_{loss}(15 nrad) [%/h]	
	damper on	damper off
6	13	17
12	9	10
24	8	9

BSRT emittance from LHC logging database (Gaussian fit)

In the LHC logging database the 1σ standard deviation $\sigma_{\text{profile},z}$ is calculated from a Gaussian fit to the horizontal and vertical projection of the BSRT image, the BSRT

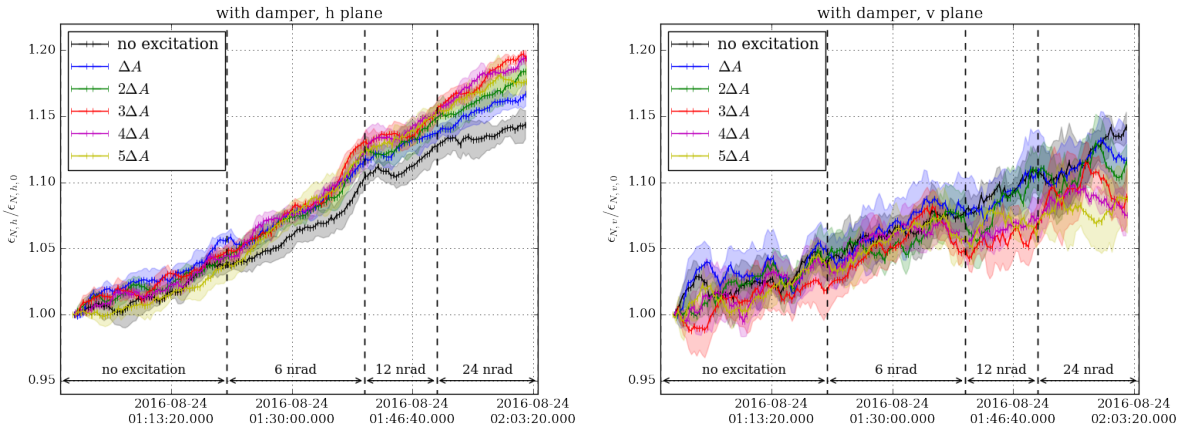

Figure 13: 7th turn pulsing H: relative emittance in the horizontal (left) and vertical (right) plane measured with the BSRT (Gaussian fit) and as defined in Eqn. 21 together with the 1σ standard deviation over the bunches with the same excitation amplitude $n{\cdot}\Delta A$ indicated as an envelope for each amplitude. For all emittance values a moving average over 10 time stamps is performed. A very small dependence of the horizontal emittance growth on the excitation amplitude $n \cdot \Delta A$ is visible. As the difference is very small, it is however debatable if this dependence is statistically relevant. The large emittance increase in the horizontal plane around 01:42:00 is partly artificial as it originates from the strong decrease of the BSRT profile background, which is probably an instrumental effect (see Fig. 14).

profiles. The sigma of the beam distribution $\sigma_{\mathrm{bunch},z}$ can then be calculated from $\sigma_{\mathrm{profile},z}$ and the correction factor from the system optical resolution $c_{\mathrm{LSF},z}$ ("LSF factor"):

$$\sigma_{\mathrm{beam},z} = \sqrt{\sigma^2_{\mathrm{profile},z} - c^2_{\mathrm{LSF},z}}, \quad z = h, v. \tag{19}$$

From the beam sigma $\sigma_{\mathrm{beam},z}$ the normalized emittance can then be obtained via the well known formula:

$$\epsilon_{N,\mathrm{bunch},z} = \beta_{\mathrm{rel}}\gamma_{\mathrm{rel}}\frac{\sigma^2_{\mathrm{beam},z}}{\beta_{\mathrm{BSRT},z}}, \quad z = h, v, \tag{20}$$

where β_{rel},γ_{rel} are the relativistic β and γ, and $\beta_{\mathrm{BSRT},z}$ is the beta function at the location of the BSRT as given in the LHC logging data base.

In order to reduce the noise, a moving average over 10 consecutive data points per bunch is taken denoted with $\langle\rangle_{10}$ in Eqn. 21. The obtained emittance is then normalized in respect to the initial emittance and then averaged over the batch of four bunches experiencing the same excitation amplitude denoted with $\langle\rangle_{\text{bunches with } n{\cdot}\Delta A}$. In summary, this yields

$$\epsilon_{N,z}(n \cdot \Delta A) = \left\langle \frac{\langle \epsilon_{N,\mathrm{bunch},z} \rangle_{10}}{\langle \epsilon_{N,\mathrm{bunch},z,0} \rangle_{10}} \right\rangle_{\text{bunches with } n{\cdot}\Delta A}, \quad z = h, v. \tag{21}$$

The emittance obtained with this method is shown in Fig. 13. A very small dependence of the horizontal emittance growth on the excitation amplitude $n \cdot \Delta A$ is visible. In the vertical plane no dependence on the excitation amplitude $n \cdot \Delta A$ nor maximum excitation amplitude A_{max} is observed. Thus the amplitude dependent emittance growth

occurs in the same plane in which the excitation is applied. As the difference is very small, it is however debatable if this dependence is statistically relevant.

BSRT profiles

In summary, the FBCT and BSRT emittance measurements showed strong excitation amplitude dependent losses and no or only a very small excitation amplitude dependent emittance growth. Furthermore, the simulations revealed an initial adjustment of the distribution in the *horizontal* plane with a depletion of the core and an increase of the population for amplitudes larger than 2.0 σ (see the residual in Fig. 4) with a peak around 3.0 σ and up to the highest amplitudes tracked, here around 5.0 σ (see the plot of the ratio in Fig. 4).

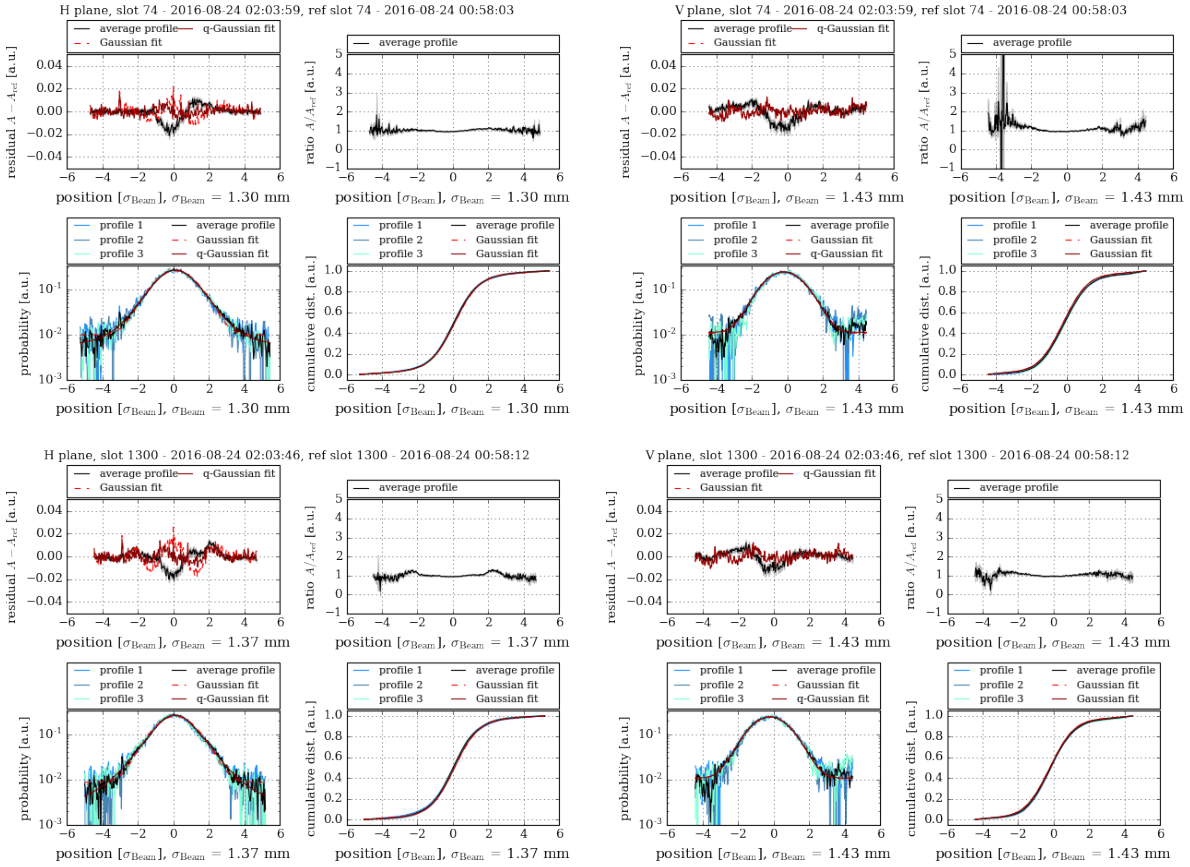

Figure 14: 7th turn pulsing H: exemplary BSRT profile for the horizontal (left) and vertical (right) plane of one reference bunch (top) and a bunch with maximum excitation (bottom) at the end of the 7th turn pulsing H and well after the change in distribution at around 01:30. The change in distribution in the horizontal and vertical plane is observed for all bunches, explicitly the ones with and without excitation and with transverse damper not active and active. The residual and ratio are taken in respect to a profile before the change in distribution (2016-08-24 01:00:15). The background is not subtracted and the moving average profiles over 11 time stamps (33 profiles) are shown.

As mentioned earlier, a change in beam distribution in the horizontal plane for all bunches is observed, starting at around 01:20 and lasting until the end of the fill. A direct comparison of the evolution of the distribution and residual for bunches with and without excitation is therefore difficult, in particular as the change in distribution is similar to the one expected from the excitation, a depletion of the core in the horizontal plane (see Fig. 14 exemplary for all bunches). As will be shown later in this section, a detailed analysis of the q-Gaussian fit however revealed a dependence of the change in distribution on the excitation amplitude.

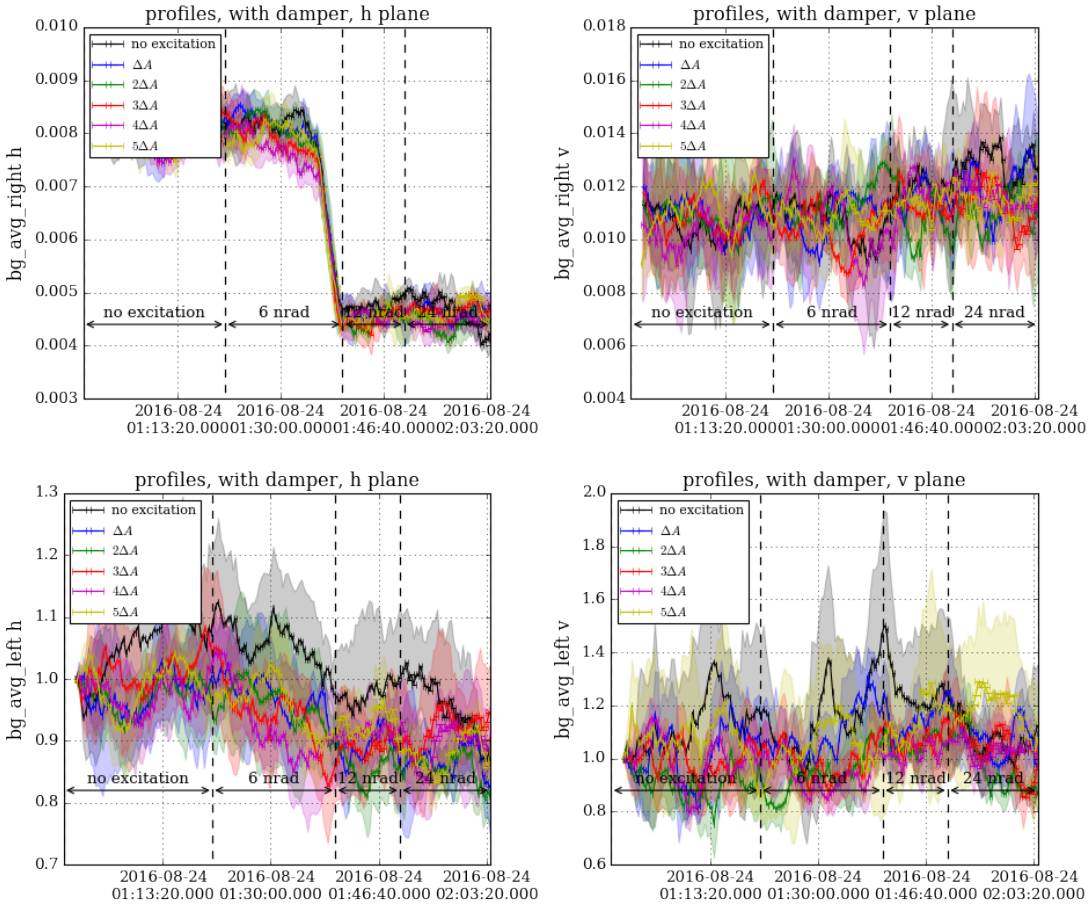

Figure 15: 7th turn pulsing H: estimate of background in the horizontal (left) and vertical (right) for the bunches with transverse damper active and before background subtraction. Estimate of the background on the right side of the profile (bg_avg_right) is shown on the top and left side on the bottom (bg_avg_left). Units are the amplitude of the probability distribution with integral 1. The background is estimated by averaging over the last ten bins. The 1σ standard deviation over the bunches with the same excitation amplitude $n \cdot \Delta A$ is indicated as an envelope for each amplitude $n \cdot \Delta A$. A large drop of the background level on the right side in the *horizontal* plane is observed. The same observations are made for bunches with transverse damper not active including in particular the drop of the background in the horizontal plane on the right.

In addition, a drop in background on the right side occurs around 01:42:00 for all bunches (see Fig. 15) independent of the excitation amplitude and if the damper is active

or not. For the BSRT profile analysis, the background is in general estimated by averaging the first and last ten bins over the full fill for each bunch. This constant value for each bunch is then subtracted for each bunch profile. This method is however only suited if the background stays approximately constant, which is not the case due to the drop at 01:42:00. Therefore, the background is not subtracted for the data presented in this section. The source of this drop in background is not known and could be either just instrumental or also a real change in beam distribution. This drop also explains the change in emittance around 01:42:00 in Fig. 13.

Except for the q-Gaussian fit parameters and σ, no dependence of any of the calculated parameters on the excitation amplitude could be observed. This observation is made for the bunches with transverse damper active and not active. Exemplary for both cases, the q-Gaussian fit parameters and σ for the bunches with transverse damper active are shown in Fig. 17 for the horizontal plane and Appendix A, Fig. 25 for the vertical plane. The following observations can be made:

- The distribution in the vertical plane (Fig. 16 right) is very close to a Gaussian distribution with slightly underpopulated tails as $q \in [0.94, 1.0] < 1$, while in the horizontal plane (Fig. 16 left) the tails are overpopulated and the core slightly depleted visible as $q \in [1.3, 1.4] > 1$. This observation is also valid for bunches without excitation and was also observed at injection during other fills.

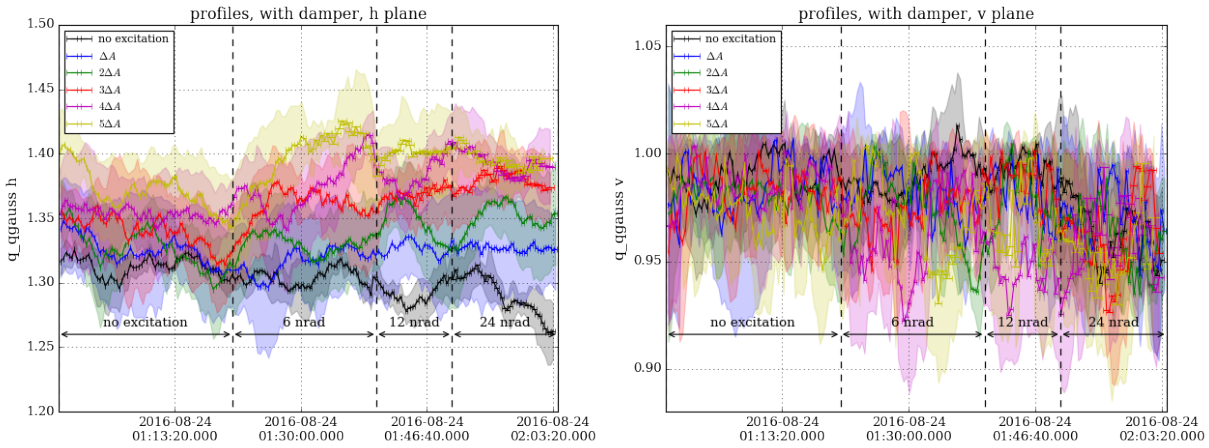

Figure 16: 7th turn pulsing H: fit parameter q from q-Gaussian fit in the horizontal (left) and vertical (right) plane for the bunches with transverse damper active. In the horizontal plane the tails are overpopulated ($q > 1$) and in the vertical plane underpopulated ($q < 1$). In the horizontal plane a clear dependence on the excitation amplitude $n \cdot \Delta A$ is visible. The fit is performed before background subtraction. The 1σ standard deviation over the bunches with the same excitation amplitude $n \cdot \Delta A$ is indicated as an envelope for each amplitude $n \cdot \Delta A$.

- In the horizontal plane, a clear dependence of the q-Gaussian fit parameters and σ on the excitation amplitude $n \cdot \Delta A$ is observed when the excitation is switched on (see Fig. 16 and 17). This indicates a change in beam distribution due to the 7th turn H pulsing. A dependence on the maximum excitation amplitude $A_{\max}$ is

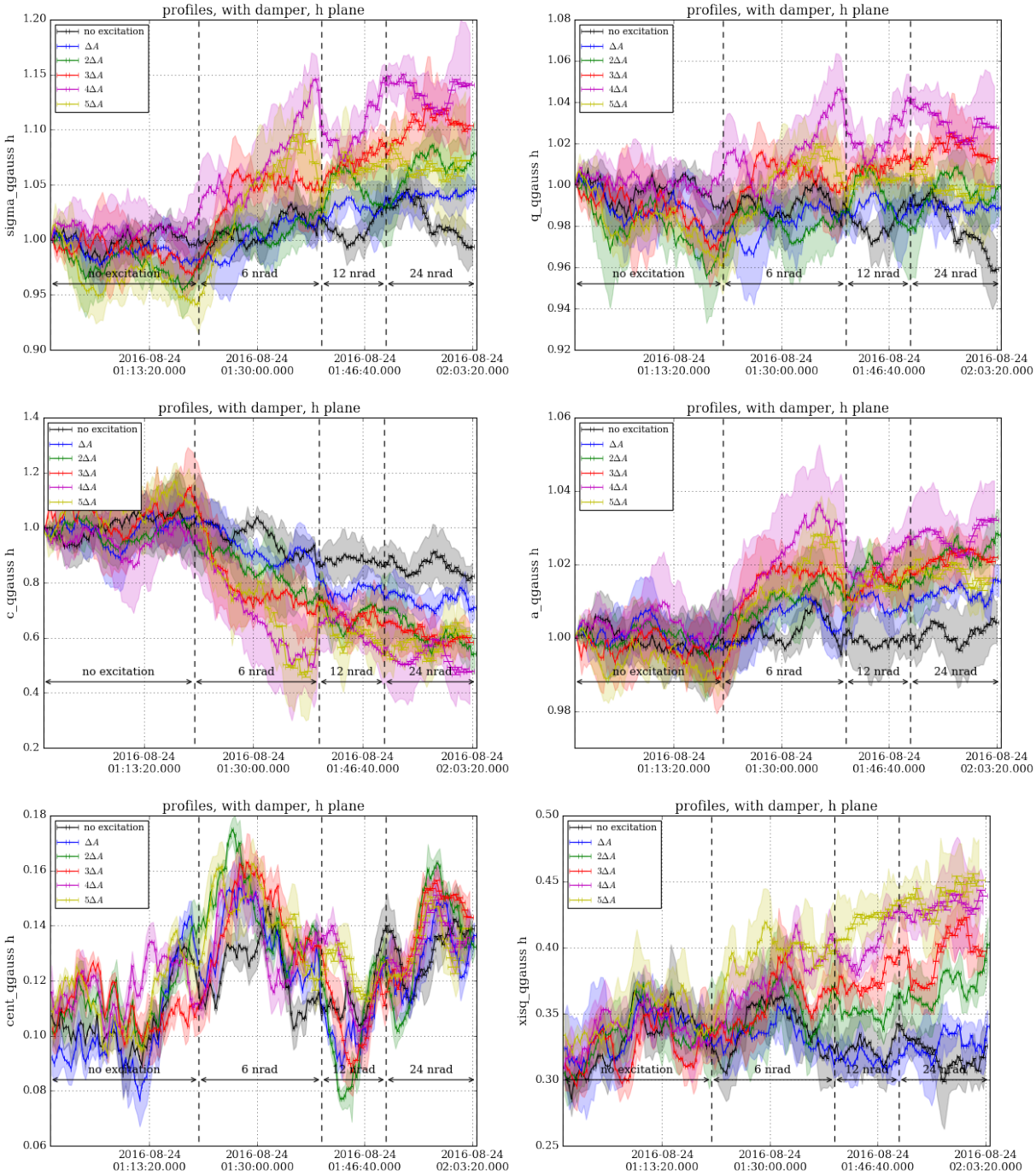

Figure 17: 7th turn pulsing H: fit parameters and σ of the q-Gaussian fit and χ^2 as measure for the goodness of the fit in the horizontal plane for the bunches with transverse damper active. The parameter cent corresponds to μ in Eqn. 7. Once the excitation is switched on a clear dependence on the excitation amplitude $n \cdot \Delta A$ is observed. A dependence on the maximum excitation amplitude $A_{\max}$ is not visible. The fit is performed before background subtraction and the parameters are normalized to the initial value. The 1σ standard deviation over the bunches with the same excitation amplitude $n \cdot \Delta A$ is indicated as an envelope for each amplitude $n \cdot \Delta A$.

however not visible. The increase of σ and small amplitude dependent increase of q indicates that the distribution in the center or middle is increasing. The decrease of c and hence increase of a (a and c are almost fully anti-correlated as shown in Appendix A, Fig. 26) suggest a depletion of the tails. This effect is also not an artifact of the fit as the correlation of the fit parameters and the χ^2 as measure for the goodness of the fit do not change considerably (see Fig. 17 and Appendix A, 26).

- In the vertical plane, the q-Gaussian fit parameters and σ do not depend on the excitation amplitude $n \cdot \Delta A$ or $A_{\max}$ (see Appendix A, Fig. 25–26)

In summary, the above observations of the changes in beam distribution agree with the simulations, in terms that a change in distribution is only observed in the horizontal plane, while the vertical plane stays unchanged. In the simulations, an increase of the high amplitude tails (above 3σ) is predicted. The q-Gaussian fit however shows a small increase in the center or middle of the distribution (increase of σ and q) and a depletion of the tails (decrease of c and increase of a). At a first glance, the simulation and measurement results thus do not agree. However, the general observation in the measurements of high losses and small emittance growth are compatible with the in simulations predicted small changes in the core region and increased tail population resulting in a higher diffusion rate for high amplitudes and thus higher loss rates.

Albeit that the fit parameters of the q-Gaussian fit show a dependence on the excitation amplitude, the data is too noisy to extract any growth rates. Also a qualitative comparison of the emittance growth with simulations fails miserably as almost no emittance growth is observed in the experiment while a strong emittance growth is seen in the simulations.

Fill 5242, 8th turn H, 3rd turn H, 3rd turn V

For pulsing every 8th turn in H, 3rd turn H and 3rd turn V the loss rate, emittance and beam distribution stay unchanged. Exemplary, the relative loss rate is shown in Fig. 18 starting from the end of the 7th turn pulsing until the end of the fill. As the initial beam distribution for these patterns was already heavily perturbed by the previous 7th turn excitation, this is however not a proof that no effect for these excitation patterns is observed. This is very vividly illustrated on the example of the 10th turn pulsing in V shown also in Fig. 18, for which only a small change is observed in fill 5242 for much higher excitation amplitudes compared to fill 5243, which starts with an unperturbed distribution. The 8th turn and 3rd turn pulsing should be therefore repeated taking an unperturbed beam distribution.

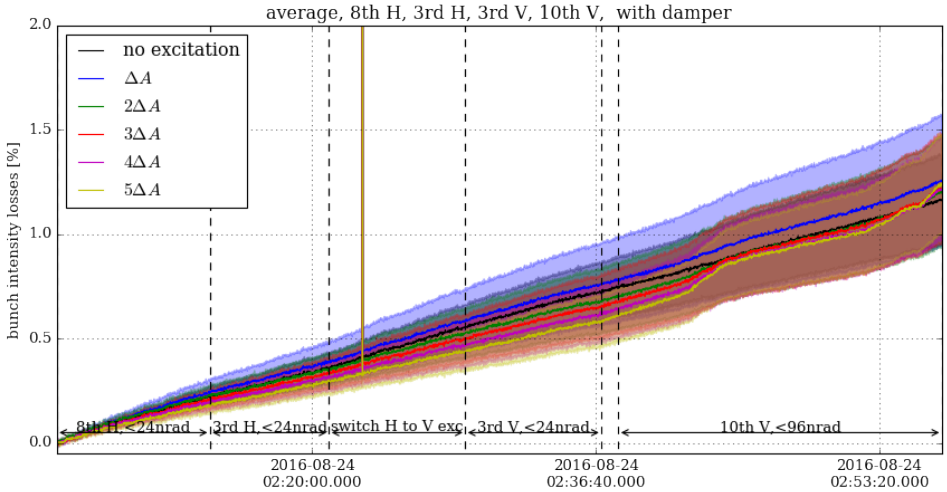

Figure 18: 8th turn H, 3rd turn H, 3rd turn V, 10th turn V: Relative bunch intensity losses measured with the FBCTs. The average over the group of four bunches experiencing the same excitation amplitude is indicated by a solid line together with the 1σ standard deviation over the four bunches indicated as an envelope in the same color. The excitation pattern and maximum excitation amplitudes are indicated with black arrows. A small increase of the losses is only observed for pulsing every 10th turn V.

Fill 5243, 10th turn V

During fill 5243 only the 10th turn pulsing V was tested for different maximum excitation amplitudes A_{max}. In summary, a strong change in beam distribution was observed together with clear amplitude dependent losses and emittance growth. In contrast to fill 5242, the reference bunches also stayed fairly stable during the entire the fill. Note that the bunches with transverse damper active and the highest excitation amplitude $5\Delta A$ were injected in the wrong bucket and thus did not experience any excitation (yellow curve in all figures with transverse damper active).

Losses and loss rates from FBCT measurements

The loss rate measured with the FBCTs and the scaling of the loss rate with the excitation amplitude for pulsing every 10th turn V are shown in Fig. 19–20. The following observations can be made:

- the loss rate depends quadratically on the excitation amplitude $n \cdot \Delta A$ (as also observed for 7th turn H),
- the loss rate decrease with the maximum excitation amplitude A_{max} (as also observed for 7th turn H),
- the loss rates for 10th turn V are in general smaller than for 7th turn H as also predicted in simulations (see Fig. 7).

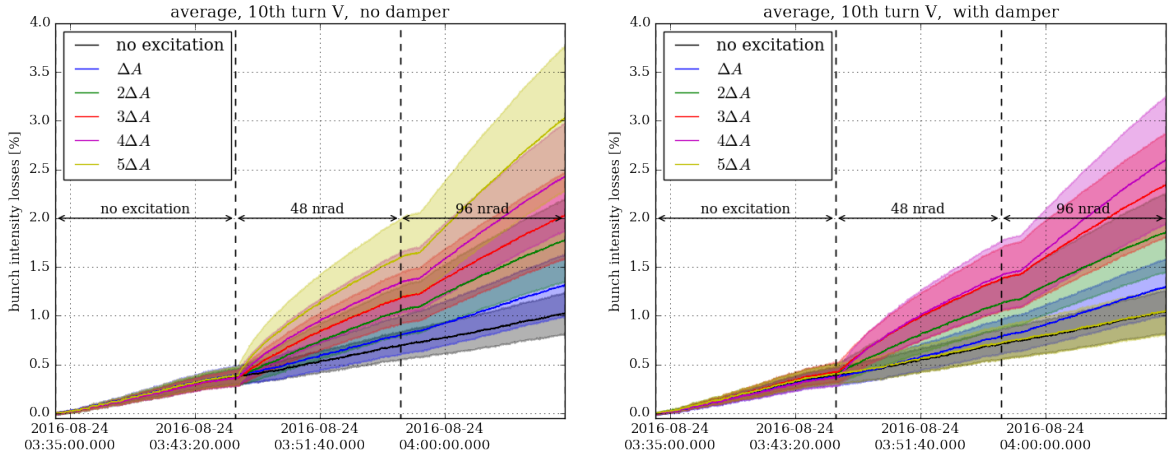

Figure 19: 10th turn pulsing V: Relative bunch intensity losses measured with the FBCTs. The average over the group of four bunches experiencing the same excitation amplitude is indicated by a solid line together with the 1σ standard deviation over the four bunch indicated as an envelope in the same color. The maximum excitation amplitudes are indicated with black arrows. A clear increase of the losses with excitation amplitude within the bunch train and at each increase of the maximum amplitude is visible. For the highest amplitude and the transverse damper active (yellow curve, right plot) the four bunches were not excited as they had been injected in the wrong bucket and therefore did not lie within the set ADT excitation window.

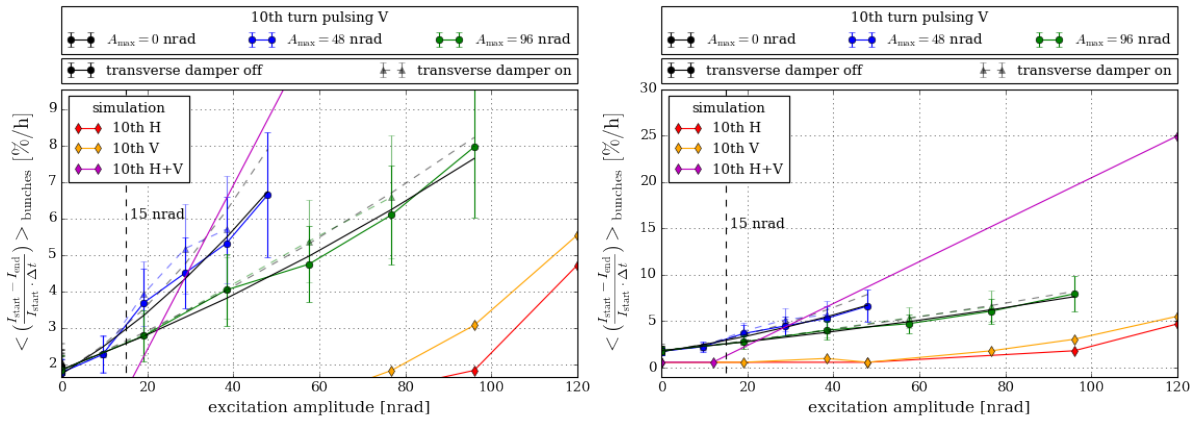

Figure 20: 10th turn pulsing V: Average bunch intensity loss rate measured with the FBCTs (Eqn. 18) together with the loss rates obtained in Lifetrac simulation (see Sec. 3.4). The left plot is a zoom of the right plot. The measurements for the different maximum excitation amplitudes $A_{\max}$ are indicated in different colors. The bunches for which the transverse damper is active are shown with solid dots and the bunches for which the transverse damper is not active are shown with slightly transparent triangles. Each point represent the average over the four bunches with the same excitation amplitude $n \cdot \Delta A$. The loss rates obtained in Lifetrac simulations are indicated with diamonds (see Sec. 3). The second order polynomial fit to the loss rate is indicated with a solid line for the bunches with transverse damper active and with a dashed line for the bunches with the transverse damper not active. The vertical dashed line at 15 nrad indicates the expected kick amplitude from the LHC electron lens [7].

- the loss rates obtained in simulations are much smaller than the loss rates obtained during the MD (as also observed for 7th turn H),

From estimates based on measurements of the 1-inch hollow electron gun prototype, the expected kick amplitude of the hollow electron lens on the core particles is [7]:

$$\theta = 15 \text{ nrad}$$

This value is indicated with a black dashed line in Fig. 20. The estimated loss rates L_{loss} from the MD using the second order polynomial fit $a + b \cdot x + c \cdot x^2$ for interpolation to 15 nrad are summarized in Table 3. The loss rates for 15 nrad lie in general around 3 %/h.

Table 3: 10th turn pulsing V: Loss rate L_{loss} as defined in Eqn. 18 for $A = 15$ nrad, the kick amplitude expected from a hollow electron lens on the core particles. The values for 15 nrad excitation amplitude are interpolated from the second order polynomial fit to the loss rate for the different maximum excitation amplitudes A_{max} (see Fig. 20).

A_{max} [nrad]	L_{loss}(15 nrad) [%/h]	
	damper on	damper off
48	3.0	2.9
96	2.6	2.6

BSRT emittance from LHC logging database (Gaussian fit)

The emittance measured with the BSRT and logged in the LHC logging database is shown in Fig. 21. The following observations can be made:

- A change of the emittance is only observed in the plane of excitation, here the vertical plane.
- Within the first 5 minutes after the excitation is switched on, a rapid, excitation amplitude dependent, increase of the emittance in the vertical plane is observed. This emittance growth is about 20% for the highest excitation amplitude $5 \cdot \Delta A = 48$ nrad. After this first rapid increase the emittance reaches an equilibrium state and does not change considerably when the maximum excitation amplitude is increased to $A_{\text{max}} = 96$ nrad. The careful analysis of the BSRT profiles showed that this change in emittance is indeed related to a change in distribution over the first 5 minutes, which then saturates afterwards. It is important to note at this point that the emittance as logged in the LHC Logging database is the σ of the Gaussian distribution fitted to the profile and is therefore model dependent. In this case, the results should be verified with a model independent estimate for the width of the distribution like the 32% or 68% of the cumulative sum or the median absolute deviation MAD as done in Sec. 4.4.3.

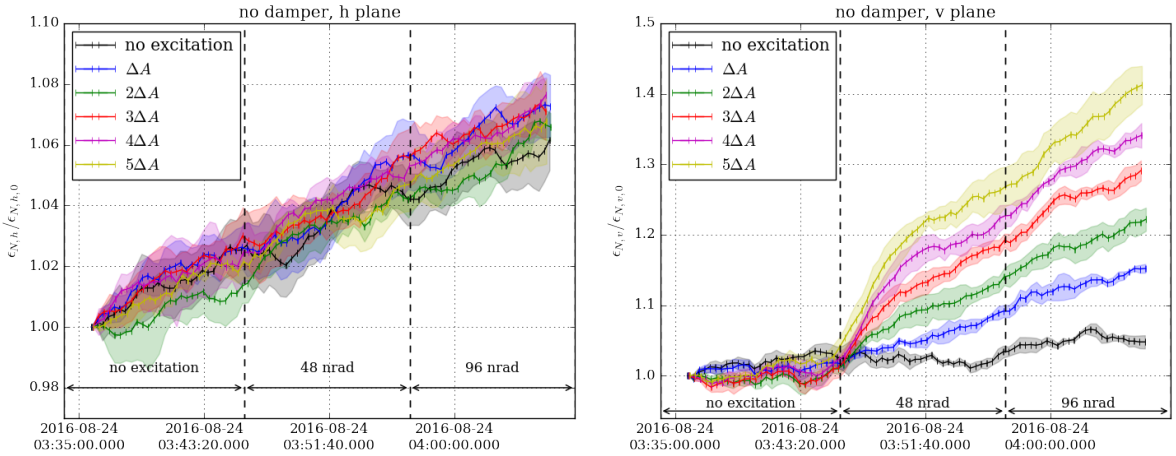

Figure 21: 10th turn pulsing V: relative emittance in the horizontal (left) and vertical (right) plane measured with the BSRT (Gaussian fit) and as defined in Eqn. 21 together with the 1σ standard deviation over the bunches with the same excitation amplitude $n{\cdot}\Delta A$ indicated as an envelope for each amplitude. For all emittance values a moving average over 10 time stamps is performed in order to reduce the noise. No emittance growth is observed in the horizontal plane. In the vertical the emittance increases rapidly over the first 5 minutes of excitation and then reaches an equilibrium state. Also the doubling of the maximum amplitude $A_{\max}$ does not seem to change this equilibrium state considerably any more.

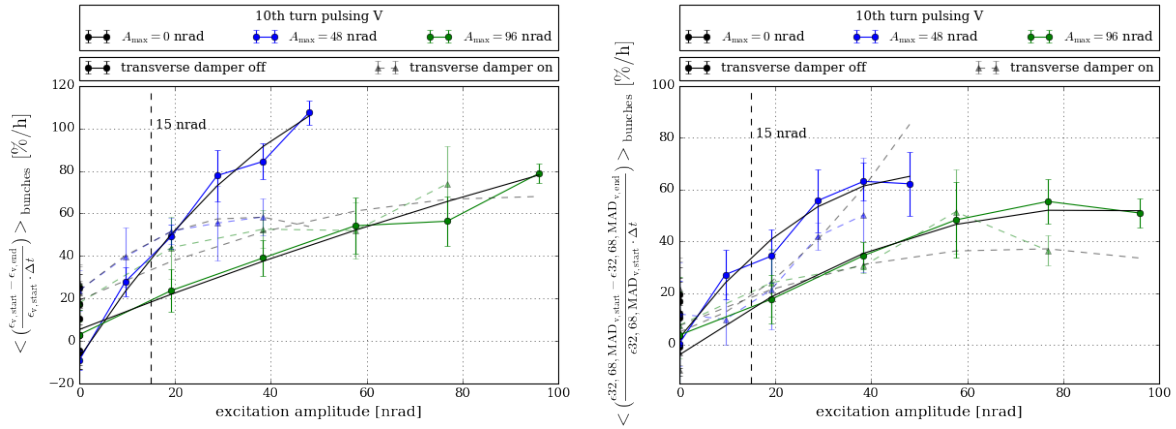

Figure 22: 10th turn pulsing V: Average emittance growth rate in the vertical plane measured with the BSRT and as defined in Eqn. 22 using the emittance ϵ from the LHC Logging database (left) or the average over the 32% cumulative sum, 68% cumulative sum and MAD $\epsilon 32, 68, \mathrm{MAD}$ (right). In the horizontal plane, no emittance growth is observed. The measurements for the different maximum excitation amplitudes $A_{\max}$ are indicated in different colors. The bunches for which the transverse damper is active are shown with solid dots and the bunches for which the transverse damper is not active are shown with slightly transparent triangles. The emittance growth rate increases approximately quadratically with the excitation amplitude $n \cdot \Delta A$. The quadratic fit to the emittance growth rate is indicated with a solid line for the bunches with transverse damper active and with a dashed line for the bunches with the transverse damper not active. The vertical dashed line at 15 nrad indicates the expected kick amplitude from the LHC electron lens [7]. For all emittance values a moving average over 10 time stamps is performed.

- Similar to the loss rate, we can define the emittance growth rate:

$$L_{\mathrm{emit},z}(n\cdot\Delta A) :=< \frac{\epsilon_{N,z,\text{start excitation}} - \epsilon_{N,z,\text{end excitation}}}{\epsilon_{N,z,\text{start excitation}}\cdot\Delta t_{\text{excitation}}} >_{\text{bunches with } n\cdot\Delta A},\ z=h,v. \tag{22}$$

  where $\epsilon_{N,z,*\text{ excitation}}$ is the normalized emittance at the start/end of the excitation. The dependence of the emittance growth rates in the vertical plane as obtained from the LHC Logging database on the excitation amplitude $n\cdot\Delta A$ and $A_{\max}$ is illustrated in Fig. 22. For comparison, also the average of the emittance calculated with the 32% cumulative sum, 68% cumulative sum and MAD $\epsilon 32, 68, \mathrm{MAD}_z$ is shown in order to have a model independent and robust estimate of the emittance. The emittance growth values from the Gaussian fit ϵ_v are in general slightly higher than the emittance $\epsilon 32, 68, \mathrm{MAD}_z$ calculated with the cumulative sum and MAD.

- within the error bars, the emittance growth rate increases quadratically with the excitation amplitude. For the Gaussian fit ϵ_v the behavior is almost linear.

Using the quadratic fit of the emittance growth rate, one then obtains for the expected kick amplitude of $\theta = 15$ nrad of the hollow electron lens on the core particles the values listed in Table 4. For comparison, the values obtained from the emittance as in the LHC Logging database $L_{\mathrm{emit},v}$ are stated together with the ones calculated with the cumulative sum, $L_{\mathrm{emit32},v}$ and $L_{\mathrm{emit68},v}$ and MAD, $L_{\mathrm{emitMAD},v}$ (see Sec. 4.4). The cumulative sum and the MAD are both model independent estimates of the emittance and the quadratic fit to the average over the three values $L_{\mathrm{emit32,68,MAD},v}$ can be considered a robust and model independent estimate of the emittance growth rate. The growth rates for $A_{\max} = 48$ nrad are in general dominated by the strong increase in emittance during the first 5 minutes of excitation and can be used as an estimate for the expected initial emittance growth. The growth rates for $A_{\max} = 96$ nrad are after the fast emittance growth and thus give

Table 4: 10th turn pulsing V: Emittance growth rate in the vertical plane as defined in Eqn. 22 for the kick amplitude expected from a hollow electron lens on the core particles $A = 15$ nrad. Either the emittance from the LHC Logging database is used $L_{\mathrm{emit},v}$ or the emittance calculated over the 32% and 68% cumulative sum, $L_{\mathrm{emit32},v}$ and $L_{\mathrm{emit68},v}$. In addition, the average of the emittance calculated over the cumulative sum and the MAD is listed in the row $L_{\mathrm{emit32,68,MAD},v}$. The values for 15 nrad excitation amplitude are interpolated from the linear fit to the emittance growth rate for the different maximum excitation amplitudes $A_{\max}$ (see Fig. 22).

$L_{*,v}$(15 nrad) [%/h]	$A_{\max} = 48$ nrad		$A_{\max} = 96$ nrad	
	damper on	damper off	damper on	damper off
$L_{\mathrm{emit},v}$	47	39	34	18
$L_{\mathrm{emit32},v}$	12	39	20	22
$L_{\mathrm{emit68},v}$	25	34	15	4
$L_{\mathrm{emitMAD},v}$	21	32	24	20
$L_{\mathrm{emit32,68,MAD},v}$	19	34	19	14

an estimate of the expected continuous emittance growth once the equilibrium state is reached. Note that for the fit for the case with damper active, only 5 values instead of 6 are used as the bunches with the highest excitation amplitude $5\Delta A$ did not experience any excitation as they were injected in the wrong bucket.

BSRT profiles

The detailed analysis of the BSRT profiles yields the following results:

- In the horizontal plane no changes in the BSRT profiles are observed consistent also with the observed emittance growth only in the vertical plane.
- The changes of the beam distribution in the vertical plane are however so dramatic, that they are plainly visible already for the smallest excitation amplitude of $1 \cdot \Delta A = 9.6$ nrad (see Appendix B, Fig. 27). During the entire excitation period, no changes are observed for the reference bunches and the changes in distribution can therefore be confidently attributed to the excitation of the bunches. Exemplary for all bunches, the moving average profiles for a bunch with $5 \cdot \Delta A$ and a reference bunch with no excitation is shown in Fig. 23. In addition the moving average profile of a bunch with $1 \cdot \Delta A$ is shown in Appendix B, Fig. 27. The profiles for the bunches with transverse damper active look very similar and no considerable benefit of the damper could be detected from the plane moving average profiles and residuals.
- The parameters of the q-Gaussian fit in the horizontal and vertical plane are shown in Appendix B, Fig. 28 and 29. In the horizontal plane a slight amplitude dependent decrease of the q-Gaussian fit parameter c is observed. This indicates a depletion of the tails in the horizontal plane. In the vertical plane, the σ of the q-Gaussian fit increases while the q-parameter decreases further. This implies that the distribution blows up in the core region while being depleted in the middle consistent with the behavior of the residual of the distribution shown in Fig. 23.
- For the emittance obtained from the LHC Logging data base (Sec. 4.4.2) the standard deviation σ of a Gaussian fit is used to calculate the emittance. In particular in the case of a distribution change as encountered for the 10th turn pulsing V, it is better to use a model independent estimate of the standard deviation σ. In this note the cumulative sum and the median absolute deviation have been used. For the cumulative sum, we define the standard deviation σ in analogy to the values for the Gaussian distribution as

$$\sigma_{32} := \mathrm{CDF}^{-1}(0.32) \tag{23}$$

$$\sigma_{68} := \mathrm{CDF}^{-1}(0.68). \tag{24}$$

  The median absolute deviation MAD is defined as

$$\mathrm{MAD}(X, W) := \mathrm{median}\left(\left|X - \mathrm{median}\left(X, W\right)\right|, W\right) \tag{25}$$

  where X is a data set and W the corresponding weights, in our case the bins and amplitude of the profile. Assuming a normal distribution, the standard deviation of the distribution is then given by:

$$\sigma = 1.4826 \cdot \mathrm{MAD}(X, W) \tag{26}$$

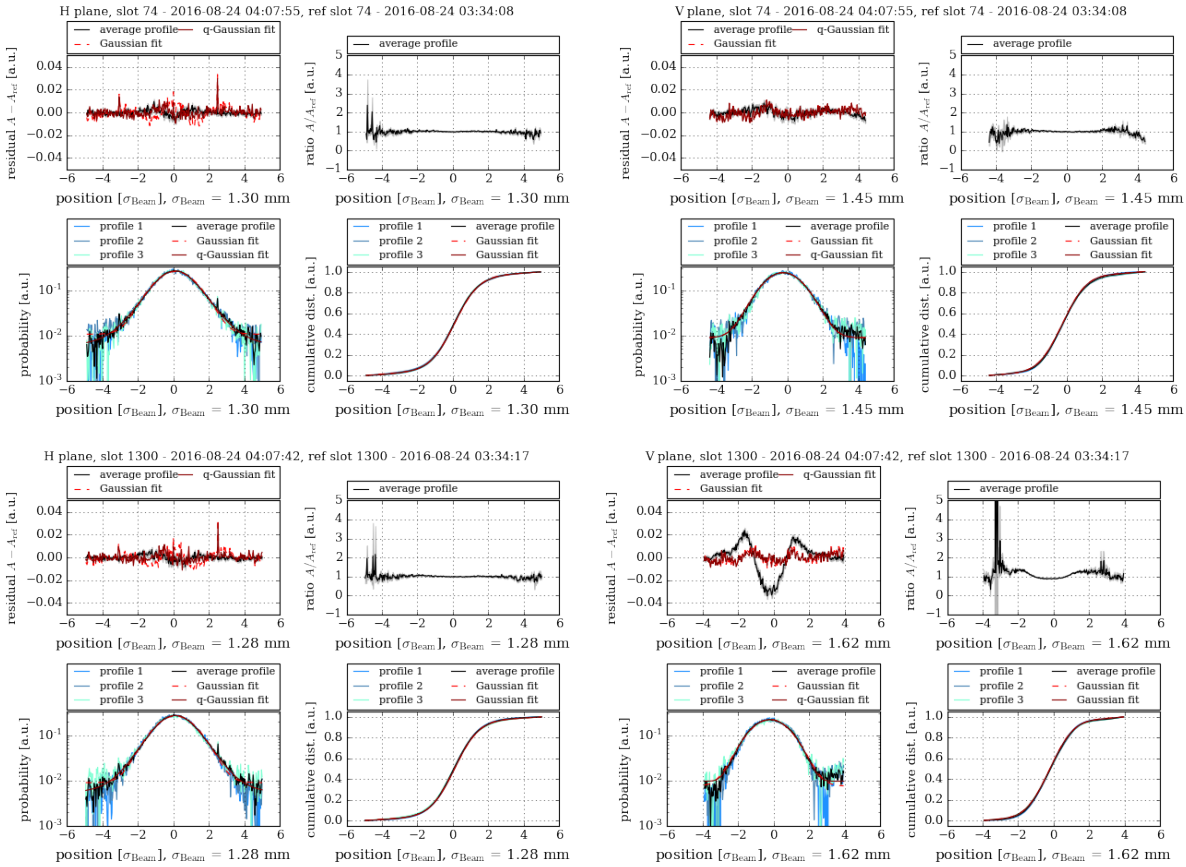

Figure 23: 10th turn pulsing V: exemplary BSRT profile for the horizontal (left) and vertical (right) plane of one reference bunch (top) and a bunch with maximum excitation $5 \cdot \Delta A$ (bottom) at the end of the 10th turn pulsing V. The beam distribution for the reference bunch stays unchanged while a depletion of the core and an increase in the middle of the distribution is observed for the excited bunch. This change is also already visible for the smallest excitation amplitude of $1 \cdot \Delta A$. The residual and ratio are taken in respect to a profile well before the excitation is switched on. The background is not subtracted and the moving average profiles over 11 time stamps (33 profiles) are shown.

Both parameters are shown for the bunches with transverse damper not active in Fig. 24 representative for also the bunches with transverse damper active. Using these two model independent estimates for the standard deviation and thus emittance, the same behavior as for the emittance calculated with the Gaussian fit is observed. This confirms that the growth is indeed real and not an artifact of the model.

Using this model independent estimate of the emittance, the growth rates shown in Fig. 22 and the estimate for an excitation amplitude of 15 nrad, the expected kick of the e-lens on the core, listed in Table 4 are obtained. For further details see Sec. 4.4.2.

In summary, the above observations of the changes in the beam distribution agree with the simulations, where an decrease of the distribution in the core region and an increase

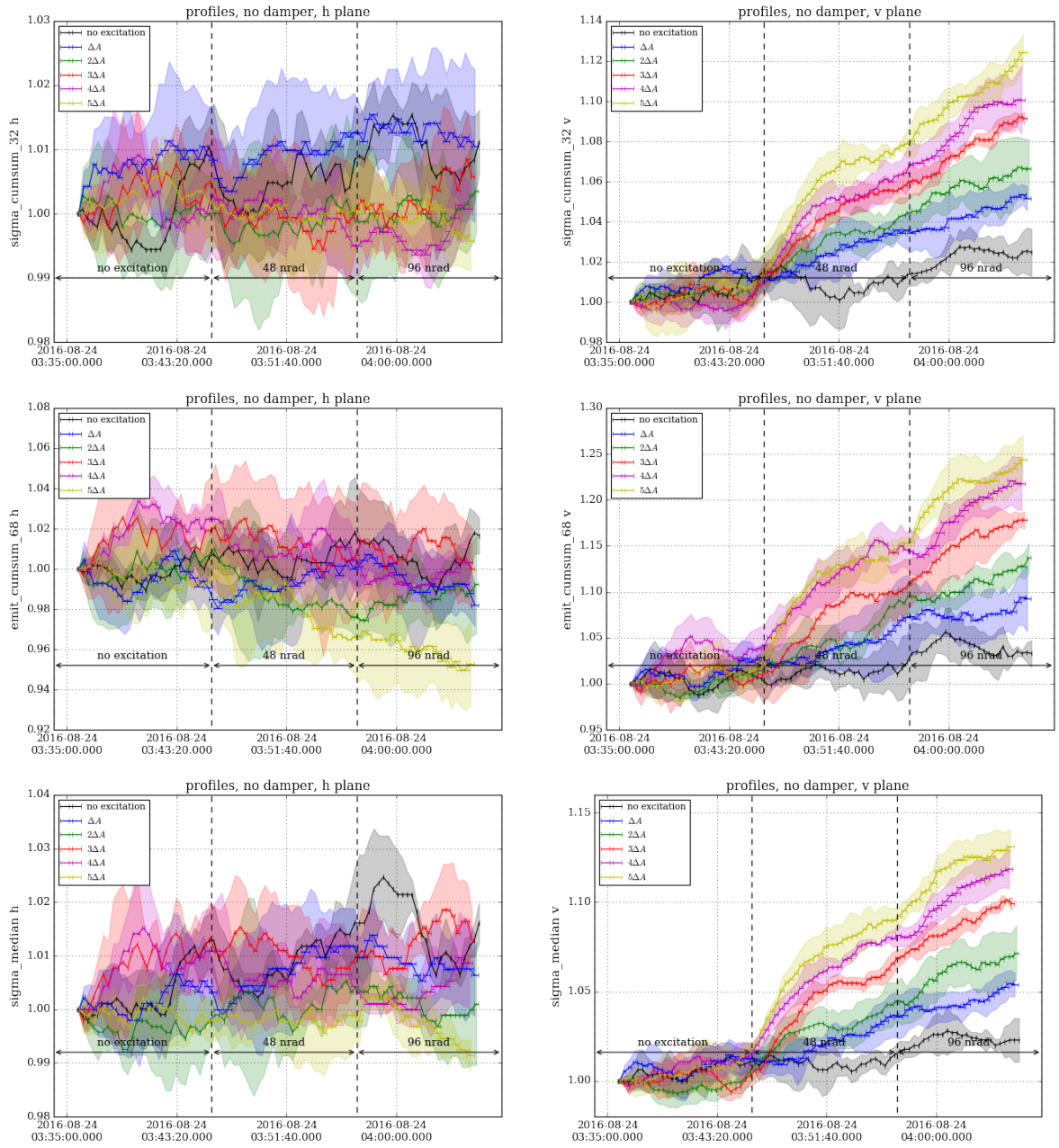

Figure 24: 10th turn pulsing V: relative standard deviation σ of the BSRT profile distribution in the horizontal (left) and vertical (right) plane. The standard deviation is calculated using the cumulative sum (top and middle) and the MAD (bottom) in order to have three model independent estimates. For all σ values a moving average over 10 time stamps is performed in order to reduce the noise and for each time stamp the average profile (over 3 profiles) is used. The 1σ standard deviation over the bunches with the same excitation amplitude $n \cdot \Delta A$ indicated as an envelope for each amplitude.

in the middle is seen in the vertical plane, while the horizontal plane stays unchanged (see Fig. 8). A qualitative comparison of the emittance growth however fails as in the simulations the emittance increases during the first second and then decreases, which is definitely not observed in the measurements.

Conclusions

The ultimate aim of this MD was to define tolerances on the kick of the e-lens on the particles in the beam core for HL-LHC in case of a pulsed operation. The main purpose of this first exploratory MD was to benchmark the simulations with beam measurements and to obtain a ballpark number for the kick amplitudes the LHC beam is sensitive to which can then be used as an upper limit for HL-LHC expected to be more sensitive to distortion than the LHC. In this MD only the resonant mode, pulsing every nth turn, was tested. Explicitly two pulsing patterns for which the maximum effect on the beam was expected based on simulations (7th turn and 10th turn pulsing) and two pulsing patterns for which no effect was expected (3rd turn pulsing and 8th turn pulsing) were tried. For the resonant mode, the MD yielded the following results:

- For the pulsing patterns 8th turn H, 3rd turn H and 3rd turn V no effect in terms of losses, emittance growth or distribution change was observed. These results have to be confirmed by a repetition of the experiment as the beam distribution was already too perturbed after the 7th turn H pulsing to make any definitive conclusions.
- For 7th turn pulsing H high losses and small emittance growth are observed.
- For 10th turn pulsing V small losses and a large emittance growth are observed.
- A comparison of the loss rates for 7th turn pulsing H and 10th turn pulsing V, yield that the simulations underestimate the observed loss rates heavily including also the approximately 50% error on the excitation amplitude in the experiment. The simulations however predicted correctly that the loss rate for 7th turn pulsing H is

Table 5: Loss rate L_{loss} as defined in Eqn. 18 for the kick amplitude $A = 15$ nrad as expected from a hollow electron lens on the core particles. The values for 15 nrad excitation amplitude are extrapolated/interpolated from the second order polynomial fit to the loss rate for the different pulsing patterns and maximum excitation amplitudes A_{max}.

excitation pattern	A_{max} [nrad]	L_{loss}(15 nrad) [%/h]	
		damper on	damper off
7th turn H	6	13	17
	12	9	10
	24	8	9
10th turn V	48	3.0	2.9
	96	2.6	2.6

higher than for 10th turn pulsing V. The loss rates scale for both pulsing patterns quadratically with the excitation amplitude $n \cdot \Delta A$. The interpolation with the quadratic fit yields the loss rates listed in Table 5 for the expected kick of 15 nrad exhibited by the e-lens on the core particles.

- In the MD, the emittance either stays unchanged or increases, while in the simulations the emittance increases initially then decreases due to the beam losses. Therefore a comparison of the simulations with the experiment already fails at this basic level. However, the plane of emittance growth, horizontal for 7th turn H and vertical for 10th turn V, was correctly predicted in simulations. For pulsing 7th turn H only the q-Gaussian fit revealed a very small increase of the emittance. For pulsing every 10th turn V the beam distribution changed considerably leading to a large emittance growth best evaluated by the average over the σ obtained from the cumulative sum and the MAD as they represent model independent estimates for the beam sigma and thus emittance. In this case the emittance growth rate also follows a quadratic behavior and the interpolation of the emittance growth rate to the kick amplitude of $A = 15$ nrad expected from the e-lens on the core particles yields the values listed in Table 6.

Table 6: 10th turn pulsing V: Emittance growth rate in the vertical plane as defined in Eqn. 22 for the kick amplitude $A = 15$ nrad expected from a hollow electron lens on the core particles. The emittance growth rate $L_{\text{emit32,68,MAD},v}$ is obtained by an interpolation of the quadratic fit to the emittance growth rate (see Fig. 22). The emittance used for the calculation of the growth rate is in this case defined as the average value of the emittance calculated via the cumulative sum and the MAD.

A_{max} [nrad]	$L_{\text{emit32,68,MAD},v}$ [%/h]	
	damper on	damper off
48	19	34
96	19	14

- The direct comparison of the residual of the BSRT profiles for pulsing 7th turn H is impeded by the change in beam distribution for all bunches, explicitly also the references bunches, taking place already during the smallest excitation amplitude of $A_{\text{max}} = 6$ nrad. Only the analysis of the q-Gaussian fit parameters showed an excitation amplitude dependent behavior. In summary, an increase of σ and q and a decrease of c as defined in Eqn. 7 were observed indicating an increase of the distribution in the center/middle and a depletion of the tails. This does not agree with the simulation results which showed an increase in the tail population together with a very small depletion in the core region. The beam distribution change predicted in the simulations is however compatible with the observation of high losses and small emittance growth indicating exactly a higher diffusion rate in the high amplitude tails (losses) and small changes in the core region (small emittance growth).

- For the 10th turn pulsing V the simulations predict a depletion of the core region and an increase of the distribution in the middle. This change is also observed in the residual of the BSRT profiles and is already visible for the smallest excitation amplitude of $1 \cdot \Delta A = 9.6$ nrad. The change occurs rather rapidly within the first 5 minutes of excitation. Afterwards, the distribution reaches an equilibrium state and does not even seem to change considerably when the maximum excitation amplitude is further increased by a factor 2, from 48 nrad to 96 nrad.

Further analysis and outlook

Except for the data acquired with the diamond BLMs and the scraping with the collimators when the beam was dumped all relevant data has been analyzed. In order to validate and extend the results of this MD, the following points should be addressed in any future measurement under the same conditions as used in this MD:

1. prediction of effective pulsing patterns: The pulsing patterns for which no effect is expected (8th turn, 3rd turn) have to be tried using an unperturbed beam distribution. Explicitly, at least before each new excitation pattern the beam should be dumped and reinjected.

2. the excitation amplitudes should be measured more precisely in order to reduce the uncertainty. This can be done before the actual MD as preparation.

3. smaller excitation amplitudes should be used in order to obtain better estimates for the kick amplitude of 15 nrad expected as kick of the e-lens on the core particles.

4. the random uniform noise should be tested for comparison with the resonant mode.

After the above points have been addressed at injection, the MD should be repeated at flat top in order to validate the obtained tolerances at 7 TeV. To repeat the MD at flat-top is particularly relevant as the tolerances on the noise induced by the e-lens are expected to be tighter than at injection.

Acknowledgements

We wish to thank the whole OP team for a succesful MD, Stéphane Fartoukh and Riccardo De Maria for their help with the preparation with the MAD-X input files and Fanouria Antoniou for her help with estimate of the intra-beam scattering growth rates and BSRT profile analysis.

References

[1] *Review on the needs for a hollow e-lens for the HL-LHC*. CERN. 2016. URL: `https://indico.cern.ch/event/567839/`.

[2] G. Stancari et al. "Collimation with Hollow Electron Beams". In: *Phys. Rev. Lett.* 107 (8 2011), p. 084802. URL: http://link.aps.org/doi/10.1103/PhysRevLett.107.084802.

[3] V. Previtali et al. *Simulation Study of Hollow Electron Beam Collimation for LHC*. Tech. rep. FERMILAB-TM-2584-APC. Fermilab, 2014. URL: http://inspirehep.net/record/1324735.

[4] V. Previtali et al. *Numerical simulations of a proposed hollow electron beam collimator for the LHC upgrade at CERN*. Tech. rep. FERMILAB-TM-2560-APC. Fermilab, 2013. URL: http://inspirehep.net/record/1247181?ln=en.

[5] M. Fitterer, G. Stancari, and A. Valishev. *Simulation Study of Hollow Electron Beam Collimation in HL-LHC*. Tech. rep. FERMILAB-TM-2636-AD. Fermilab, 2016. URL: http://inspirehep.net/record/1492682.

[6] X.-L. Zhang et al. "Generation and diagnostics of uncaptured beam in the Fermilab Tevatron and its control by electron lenses". In: *Phys. Rev. ST Accel. Beams* 11 (5 2008), p. 051002. URL: http://link.aps.org/doi/10.1103/PhysRevSTAB.11.051002.

[7] M. Fitterer, G. Stancari, and A. Valishev. *Effect of pulsed hollow electron-lens operation on the proton beam core in LHC*. Tech. rep. FERMILAB-TM-2635-AD. Fermilab, 2016. URL: http://inspirehep.net/record/1496416.

[8] J. Barranco Garcia et al. *MD 400: LHC emittance growth in presence of an external source of noise during collision*. Tech. rep. CERN-ACC-NOTE-2016-0020. CERN, 2016. URL: https://cds.cern.ch/record/2125228.

[9] *private communication G. Papotti*.

[10] D. Shatilov et al. "Lifetrac code for the weak-strong simulation of the beam-beam effects in Tevatron". In: *Conf. Proc.* FERMILAB-CONF-05-246-AD, PAC-2005-TPAT084 (2005). URL: http://inspirehep.net/record/687566/files/fermilab-conf-05-246.pdf.

[11] M. Fitterer et al. *Analysis of BSRT profiles in the LHC at injection*. Tech. rep. to be published. Fermilab, 2017.

Additional figures for fill 5242, 7th turn pusling H

q-Gaussian fit parameters in the vertical plane

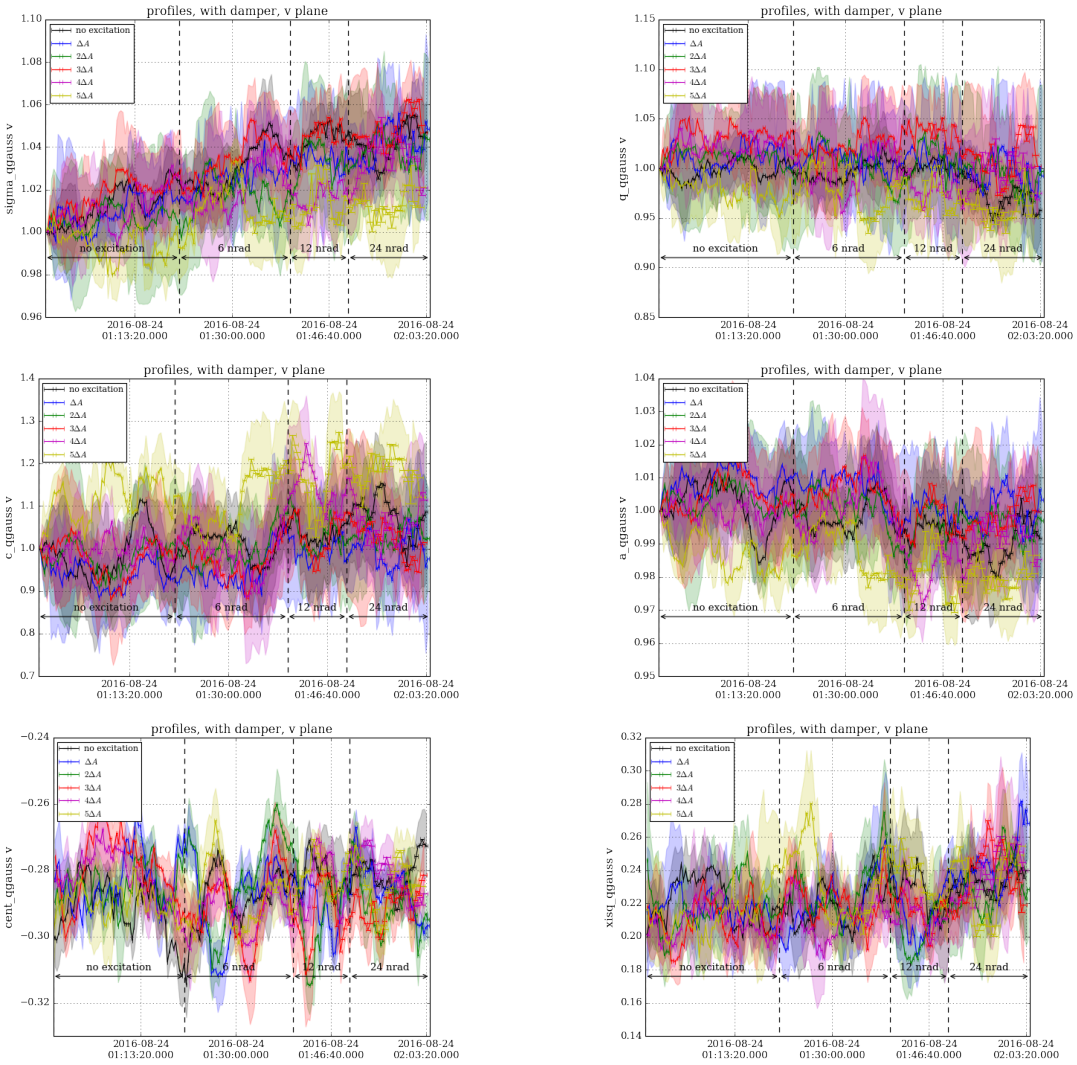

Figure 25: 7th turn pulsing H: q-Gaussian fit parameter, σ and χ^2 as measure for the goodness of the fit in the vertical for the bunches with transverse damper active. No dependence of the fit parameters, on the excitation amplitude $n{\cdot}\Delta A$ or $A_{\max}$ is observed in the *vertical* plane. The fit is performed before background subtraction and the parameters are normalized to the initial value. The 1σ standard deviation over the bunches with the same excitation amplitude $n \cdot \Delta A$ is indicated as an envelope for each amplitude $n \cdot \Delta A$.

Correlation of q-Gaussian fit parameters and χ^2

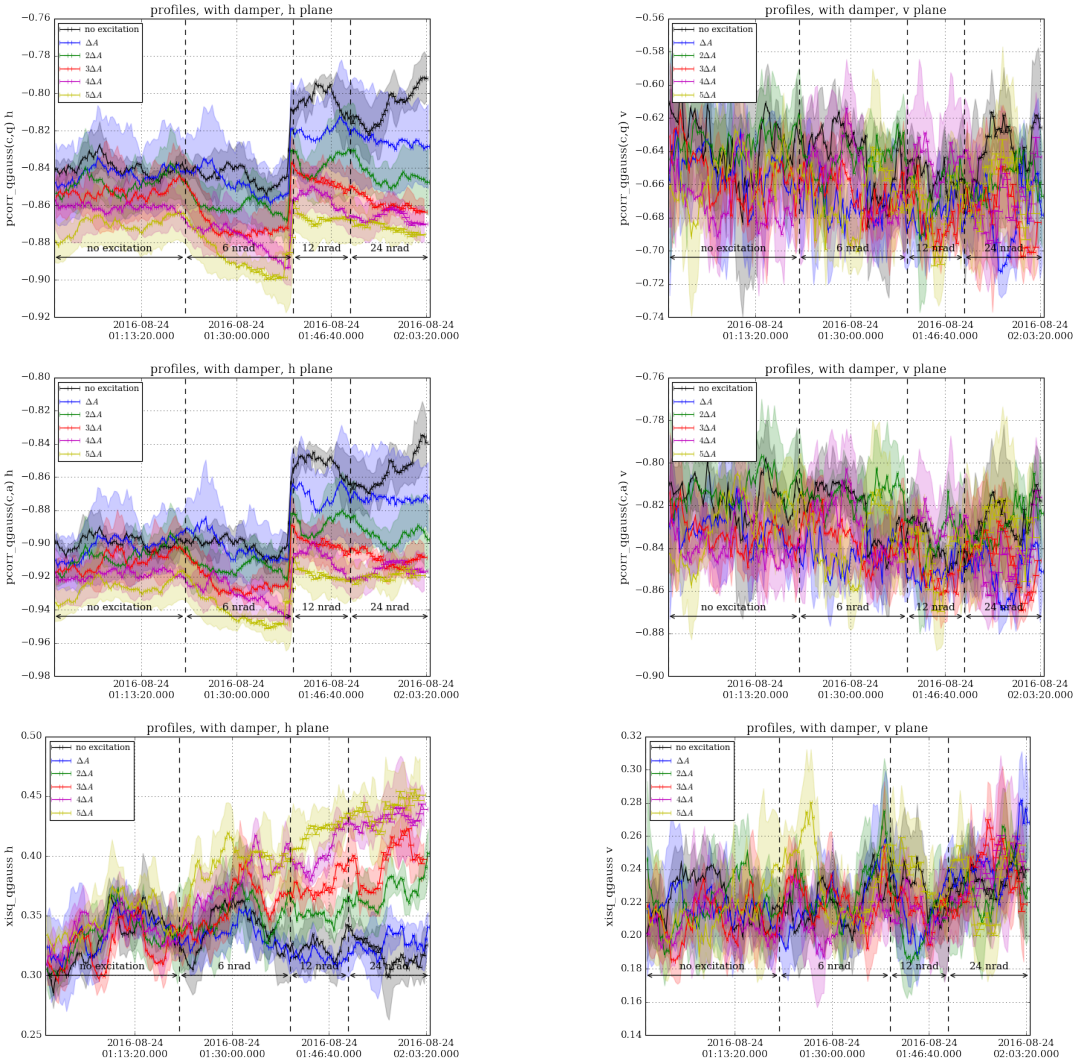

Figure 26: 7th turn pulsing H: correlation between fit parameter c, q and a of q-Gaussian fit and calculated normalized ξ^2 for bunches with transverse damper active. Except for the jump when the background on the right side in the horizontal increases, the correlation stays almost constant. The increase in ξ^2 however indicates a decrease of the goodness of the fit. The fit is performed before background subtraction and the parameters are normalized to the initial value. The 1σ standard deviation over the bunches with the same excitation amplitude $n \cdot \Delta A$ is indicated as an envelope for each amplitude $n \cdot \Delta A$.

Additional figures for fill 5243, 10th turn pulsing V

BSRT profile for bunch with $1 \cdot \Delta A$

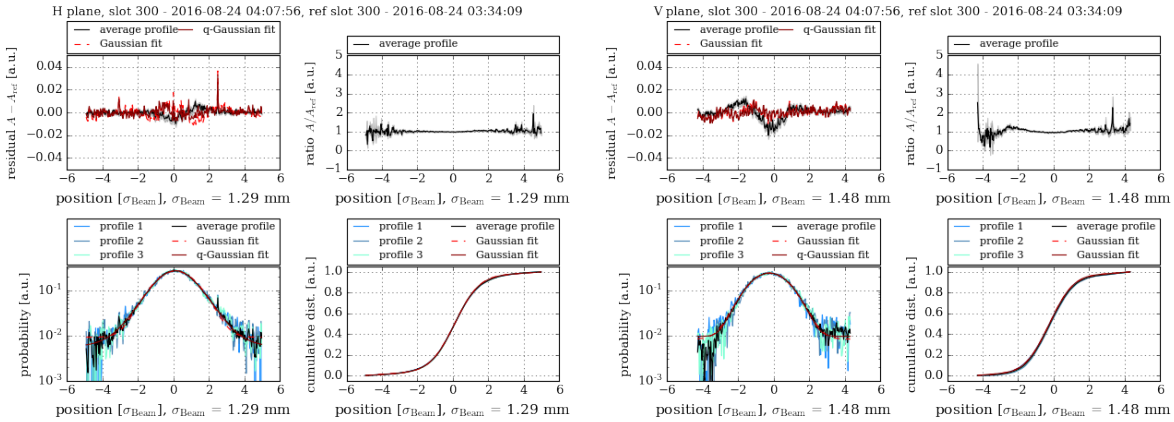

Figure 27: 10th turn pulsing V: exemplary BSRT profile for the horizontal (left) and vertical (right) of a bunch with maximum excitation $1 \cdot \Delta A$ at the end of the 10th turn pulsing V. The residual and ratio are taken in respect to a profile well before the excitation is switched on. The background is not subtracted and the moving average profiles over 11 time stamps (33 profiles) are shown.

q-Gaussian fit parameters in the horizontal plane

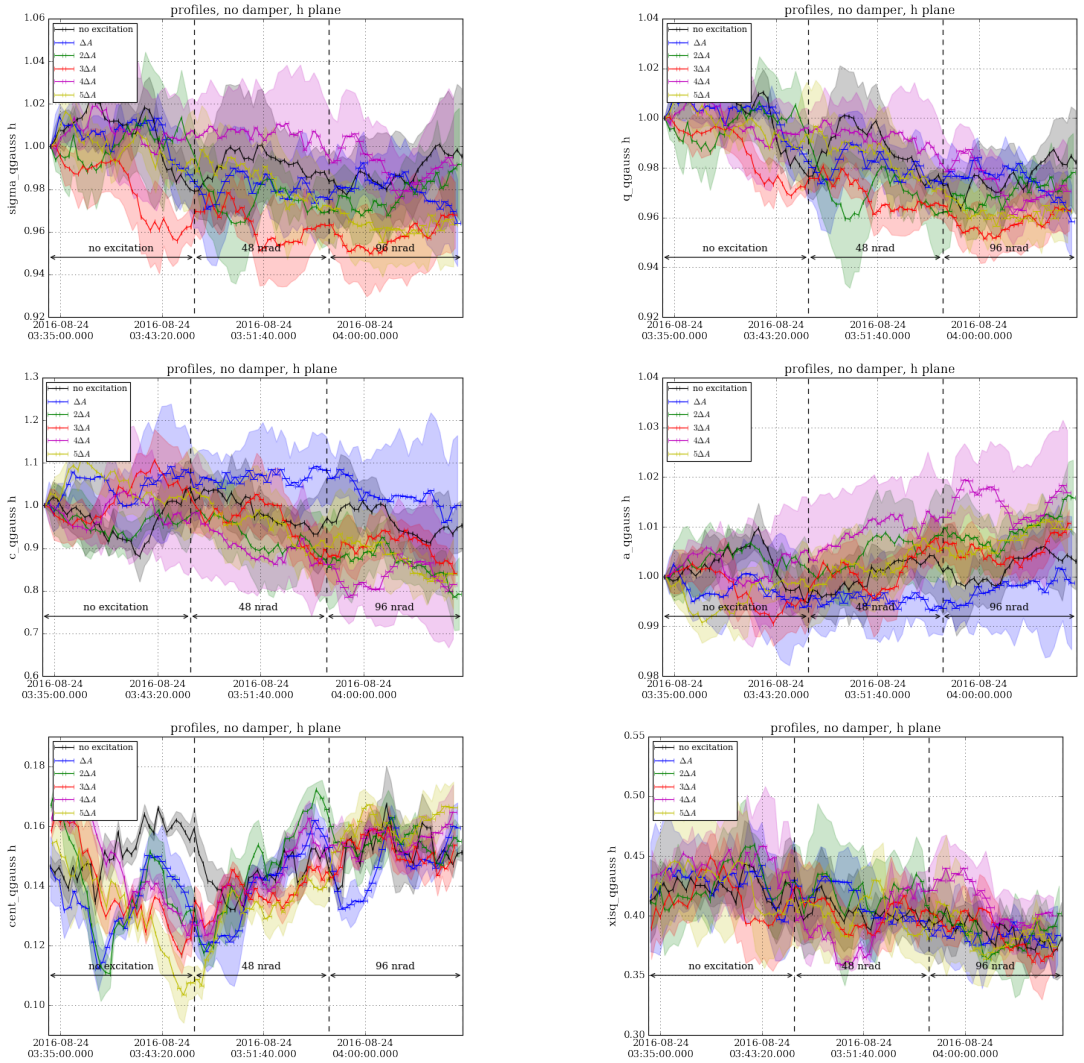

Figure 28: 10th turn pulsing V: fit parameter q (top) and calculated χ^2 (bottom) for the q-Gaussian fit in the horizontal (left) and vertical (right) plane for the bunches with transverse damper not active. The fit is performed before background subtraction and on the moving average profiles taking 10 time stamps (33 profiles). The 1σ standard deviation over the bunches with the same excitation amplitude $n \cdot \Delta A$ is indicated as an envelope for each amplitude $n \cdot \Delta A$.

q-Gaussian fit parameters in the vertical plane

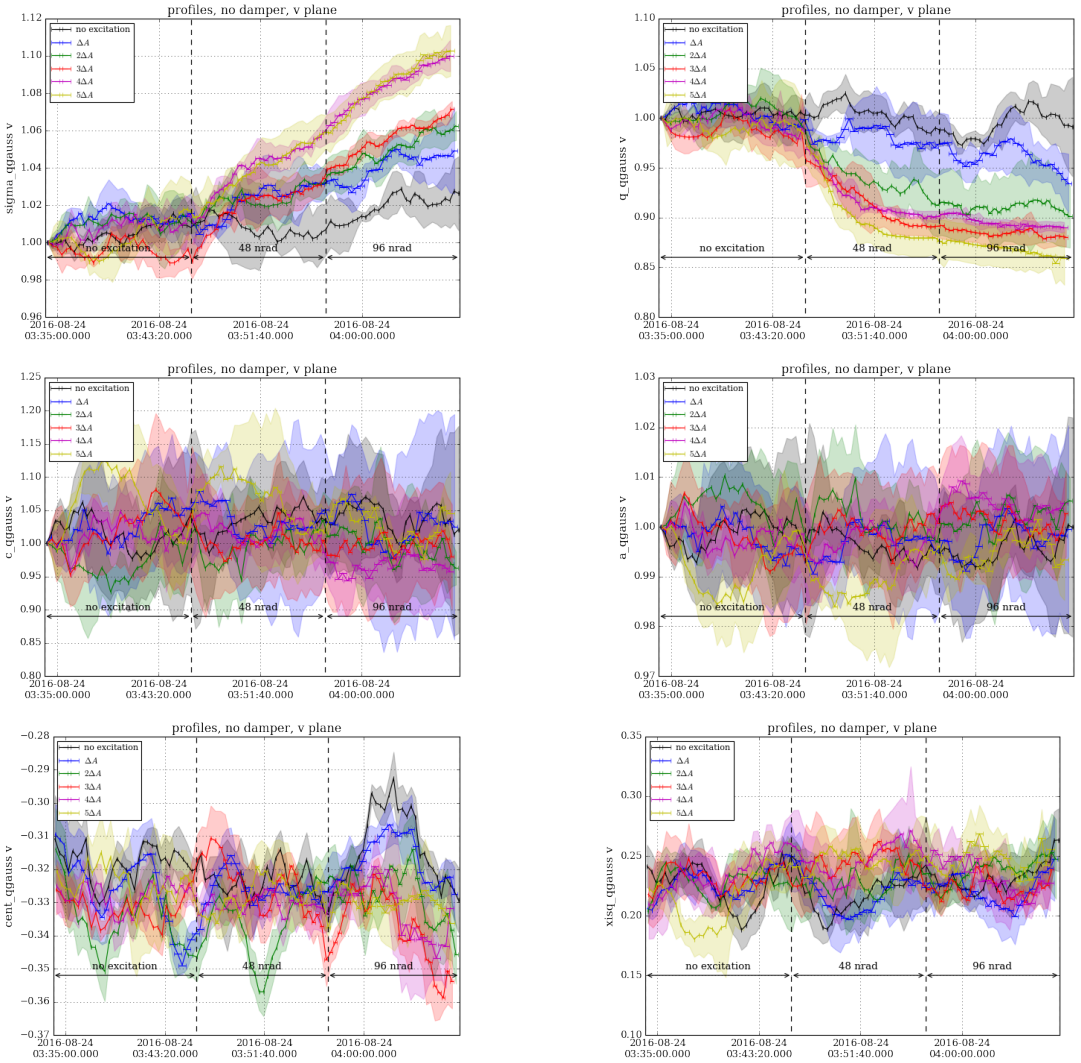

Figure 29: 10th turn pulsing V: fit parameter q (top) and calculated χ^2 (bottom) for the q-Gaussian fit in the horizontal (left) and vertical (right) plane for the bunches with transverse damper not active. The fit is performed before background subtraction and on the moving average profiles taking 10 time stamps (33 profiles). The 1σ standard deviation over the bunches with the same excitation amplitude $n \cdot \Delta A$ is indicated as an envelope for each amplitude $n \cdot \Delta A$.